Mathematical Biosciences and Engineering

https://www.aimspress.com/journal/mbe

MBE, 23(11): 3273–3319.
DOI: 10.3934/mbe.2026113
Received: 01 August 2026
Revised: 17 October 2026
Accepted: 29 October 2026
Published: 04 November 2026

Research article

Dynamic analysis and optimal control of a plant–pest model with dual transmission and allomone effects

Taufan Talib[1,2], Agus Suryanto[1,*], Isnani Darti[1] and Wuryansari Muharini Kusumawinahyu[1]

[1] Department of Mathematics, University of Brawijaya, Jalan Veteran, Malang 65145, Indonesia

[2] Department of Mathematics Education, University of Pattimura, Jalan Ir. M. Putuhena, Ambon 97233, Indonesia

* **Correspondence:** Email: suryanto@ub.ac.id.

Abstract: We develop an eco-epidemiological model consisting of susceptible plant biomass, infected plant biomass, and pest density. The pest density plays a dual role by feeding on plant biomass and contributing to effective vector-mediated disease transmission. Allomone effects are included to reduce the net contribution of susceptible and infected plant consumption to pests' growth. The model accounts for direct plant-to-plant transmission, vector-mediated transmission, herbivory, and chemical plant defense. We analyze the existence and uniqueness, non-negativity, boundedness, equilibrium points, invasion thresholds, and local stability. The Li–Muldowney geometric approach is used to study the global stability of the coexistence equilibrium. A transcritical bifurcation characterizes the threshold transition in the direct transmission dynamics on the pest-free invariant subspace, while a codimension-two threshold interaction occurs when the direct transmission and pest density invasion thresholds are simultaneously satisfied. A Hopf bifurcation indicates the onset of oscillatory coexistence, and numerical simulations further show how vector-mediated transmission can amplify long-term fluctuations. The Latin hypercube sampling (LHS) and partial rank correlation coefficients (PRCCs) sensitivity results identify direct transmission, infected-plant removal, carrying capacity, and pest mortality as important parameters associated with the long-term mean state variables, with pest mortality showing the strongest association with mean pest density. The simulations also show that allomone-mediated pest suppression can reduce pest density and stabilize coexistence. An optimal control problem with treatment and insecticide interventions is then formulated and characterized through Pontryagin's minimum principle. For the selected objective function weights and control bounds, the combined treatment–insecticide strategy provides the strongest reduction in infected plant biomass and pest density among the scenarios considered, while maintaining susceptible plant biomass near the carrying capacity.

Keywords: allomone effects; bifurcation; optimal control; plant disease; vector-mediated transmission

1. Introduction

Plant pests and diseases reduce agricultural productivity by lowering crop yield and quality, increasing management costs, and disturbing agroecosystems' stability [1, 2]. Chemical pesticides are widely used because they act quickly, but their overuse can lead to residues, pest resistance, harmful impacts on nontarget organisms, and long-term ecological hazards [1–6]. These concerns have motivated the development of mathematical models that relate disease transmission, pest population dynamics, and more sustainable control measures.

Pest insects feed on plant tissues and cause substantial damage in agricultural systems while also acting as vectors for plant infections. The resulting system couples ecological interactions, through herbivory, with epidemic processes, since pathogen transmission changes plants from susceptible to infected states [7–11]. An eco-epidemiological framework is therefore appropriate for describing the dynamics of pest density, plant infection, and plant growth within a single modeling structure. Plants' chemical defenses are important in plant–insect interactions. Plants also release secondary metabolites or volatile organic compounds that may repel insects, reduce their feeding activity, or alter host selection behavior [12–15]. Allomones are interspecific chemical signals that benefit the emitting organism by altering the behavior or performance of another organism [16–19]. In plant–pest interactions, allomones can reduce pest establishment, feeding intensity, or pest reproduction.

A biological example is provided by clove (*Syzygium aromaticum*), whose essential oil is composed of eugenol, eugenyl acetate, beta-caryophyllene, and alpha-humulene. These compounds have been reported to exhibit repellent, fumigant, insecticidal, and antifeedant properties against certain insect groups [20–23]. Generally, plant-derived defensive chemicals (e.g., azadirachtin, nicotine, glucosinolates, pyrethrins, volatile organic compounds) influence plant–insect interactions [4, 24–26]. Plant infections can also alter volatile profiles, which can influence pests' or vectors' behavior and disease dissemination [27–31].

Recent eco-epidemiological studies have shown that nonlinear interactions between ecological and epidemiological processes can generate complex dynamic behavior, including threshold-dependent transitions and bifurcation phenomena [32, 33]. Mathematical models of plant–pest–disease systems have separately addressed vector-borne pathogens' transmission [34–36], tritrophic and pest–natural-enemy interactions [37–39], and the design of disease control interventions [34, 36]. Most of these formulations, however, treat herbivory and pathogen transmission as decoupled processes or confine the vector to a purely epidemiological role, and they rarely represent plants' chemical defenses as an explicit ecological feedback on pest dynamics. In particular, a single framework that simultaneously couples (i) direct plant-to-plant transmission, (ii) vector-mediated spread, (iii) herbivory on both susceptible and infected plants, and (iv) allomone-driven suppression of pest growth remains comparatively underexplored. This gap is addressed by a three-dimensional susceptible–infected–vector model whose defining feature is a dual-role pest—acting simultaneously as a herbivore and a vector—coupled with allomone defenses that act directly to reduce the net contribution of plant consumption to pest growth. We then analyze the resulting dynamics and develop optimal control strategies combining plant treatment and insecticide application.

This paper is organized into six sections. Following this introduction, Section 2 presents the model formulation and fundamental properties. Section 3 develops the analytical results, including equilibria, invasion thresholds, local stability, persistence, global stability, bifurcation analysis, and global sensi-

tivity analysis. Section 4 provides numerical simulations and their biological interpretation, whereas Section 5 focuses on the optimal control problem with crop treatments and insecticide applications. Finally, Section 6 presents the conclusion.

2. Model formulation and fundamental properties

2.1. Model formulation

Let $S(t)$, $I(t)$, and $V(t)$ denote the susceptible plant biomass, infected plant biomass, and total pest density at time t, respectively. The pest population plays a dual ecological role: It consumes plant biomass through herbivory and contributes to pathogen transmission as a disease vector [13,40]. In the present reduced formulation, vector-mediated transmission is represented through an effective infectious pressure associated with the pest population. A schematic representation of the proposed model is shown in Figure 1.

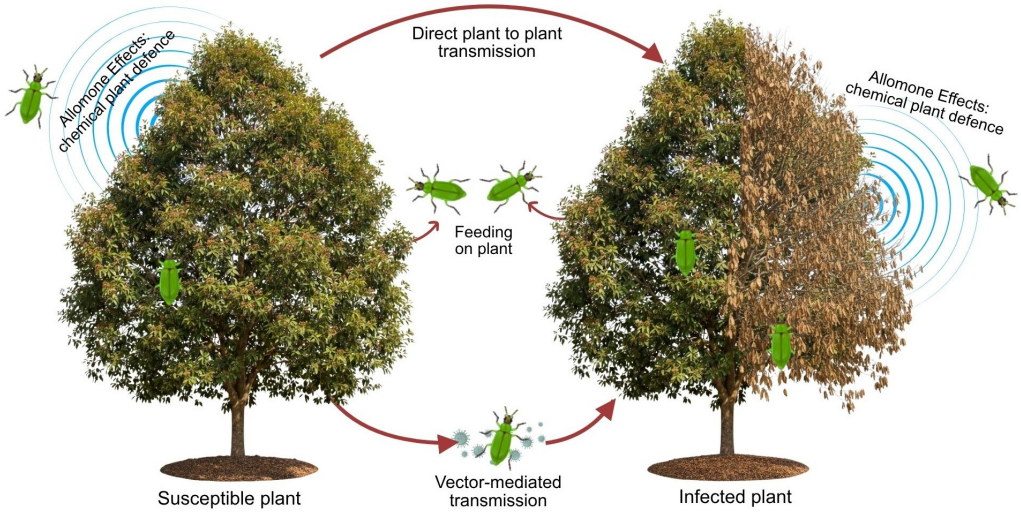


Figure 1. Schematic diagram of the plant–pest model with direct transmission, effective vector-mediated transmission, herbivory, and allomone-mediated suppression. The pest population contributes to plant damage through herbivory and to disease transmission through an effective infectious vector pressure. Allomone effects reduce the net demographic gain obtained by pests from plant consumption.

In the absence of disease and pest pressure, susceptible plant biomass is assumed to grow logistically with the intrinsic growth rate r and a carrying capacity K. Disease transmission occurs through two distinct pathways. The first pathway is direct plant-to-plant transmission, represented by $\beta_L S I$, where β_L is the direct transmission coefficient. The second pathway is pest-mediated transmission, represented by $\beta_T S V$, where β_T denotes an effective vector-mediated transmission coefficient. Thus, the total infection incidence is represented by $(\beta_L I + \beta_T V)S$.

Besides contributing to pathogen transmission, pests feed on both susceptible and infected plant biomass. The corresponding herbivory losses are represented by $a_S S V$ and $a_I I V$, where a_S and a_I denote the herbivory rates on susceptible and infected plant biomass, respectively.

Pest feeding contributes to the pest population's growth. The parameters γ_S and γ_I denote the conversion efficiencies from consumed susceptible and infected plant biomass into the pest population's growth, respectively. Susceptible and infected plants are also assumed to produce allomone-mediated chemical defenses that reduce the net demographic benefit obtained by pests from plant consumption at rates η_S and η_I, respectively [41–43].

In the present model, the allomone parameters do not directly modify the herbivory rates a_S and a_I. Instead, they reduce the net demographic gain obtained by pests from consuming plant biomass [40, 43, 44]. Therefore, η_S and η_I represent allomone-mediated suppression of the pest population's growth rather than a direct reduction in feeding intensity. Accordingly, the herbivory terms $-a_S S V$ and $-a_I I V$ remain unchanged.

We hypothesize that the allomone-mediated suppression is stronger in susceptible than in infected plants, i.e., $\eta_S > \eta_I$. This assumption reflects the possibility that healthy plants retain stronger chemical defenses, whereas infection may alter plant physiology and reduce their defensive capacity.

Assumption of effective vector-mediated transmission. In the present model, $V(t)$ denotes the total pest density, without distinguishing between infectious and noninfectious pests. Vector-mediated transmission is therefore described using an effective transmission coefficient rather than a separate infectious pest compartment.

Let $q \in [0, 1]$ represent the proportion of pests capable of transmitting the pathogen, and let $\widetilde{\beta}_T$ be the transmission coefficient per infectious pest. The resulting incidence is $\widetilde{\beta}_T(qV)S$. By setting $\beta_T = \widetilde{\beta}_T q$, this expression reduces to $\beta_T S V$. Thus, β_T accounts for both transmission efficiency and the proportion of infectious pests.

We assume that the plant–pest system is embedded in a wider agroecosystem where pathogen exposure may persist beyond the focal plant population. Consequently, infectious pests may be present even when no infected plants remain within the modeled system. The proportion q is assumed to be constant over the time scale of interest. Under this assumption, $\beta_T S V$ can remain positive when $I = 0$, provided that $S > 0$, $V > 0$, and $\beta_T > 0$. This represents the infection pressure associated with pathogen exposure outside the focal system, rather than spontaneous infection caused by noninfectious pests.

The model does not explicitly describe pathogen acquisition by pests from infected plants. Incorporating this mechanism would require separate infectious and noninfectious pest classes and would extend the present three-dimensional formulation. Accordingly, $\beta_T S V$ should be understood as an effective population-level transmission term, without assuming that all pests are infectious.

We define the net pest growth coefficients as $c_S = \gamma_S a_S - \eta_S$ and $c_I = \gamma_I a_I - \eta_I$. Accordingly, both c_S and c_I have a dimension $B^{-1}T^{-1}$, which is consistent with the pest population equation. The quantities $\gamma_S a_S$ and $\gamma_I a_I$ represent the demographic gains obtained by pests from feeding on susceptible and infected plant biomass, respectively, whereas η_S and η_I represent allomone-mediated reductions in these gains. Hence, c_S and c_I describe the effective net contribution of susceptible and infected plant biomass to the pest population's growth.

Depending on the relative magnitudes of conversion efficiency and allomone-mediated suppression, the coefficients c_S and c_I may, in principle, be positive, zero, or negative. The specific sign conditions required for pests' invasion, persistence, and coexistence are stated explicitly in the corresponding analytical results.

With these assumptions, the uncontrolled eco-epidemiological plant–pest model with direct trans-

mission, effective vector-mediated transmission, herbivory, and allomone-mediated suppression is given by

$$\begin{aligned} \frac{dS}{dt} &= rS\left(1-\frac{S+I}{K}\right)-(\beta_L I+\beta_T V)S-a_S S V,\\ \frac{dI}{dt} &= (\beta_L I+\beta_T V)S-a_I I V-d_I I,\\ \frac{dV}{dt} &= c_S S V+c_I I V-d_V V, \end{aligned} \tag{2.1}$$

The initial condition is $X(0) = X_0 = (S_0, I_0, V_0) \in \mathbb{R}^3_+$, where $S_0 \geq 0$, $I_0 \geq 0$, and $V_0 \geq 0$. The biologically relevant phase space is $\mathbb{R}^3_+ = \{(S, I, V) \in \mathbb{R}^3 : S \geq 0,\ I \geq 0,\ V \geq 0\}$.

Table 1. Biological interpretation and dimensions of the model parameters.

Parameter	Biological interpretation	Dimension
r	Intrinsic growth rate of susceptible plant biomass	T^{-1}
K	Carrying capacity for total plant biomass	B
β_L	Direct plant-to-plant transmission coefficient	$B^{-1}T^{-1}$
β_T	Effective vector-mediated transmission coefficient	$P^{-1}T^{-1}$
a_S, a_I	Herbivory rates on susceptible and infected plant biomass	$P^{-1}T^{-1}$
d_I	Removal or natural loss rate of infected plant biomass	T^{-1}
d_V	Natural mortality rate of pest density	T^{-1}
γ_S, γ_I	Conversion efficiencies from consumed plant biomass to pest growth	PB^{-1}
η_S, η_I	Allomone-mediated reductions in pests' demographic gain	$B^{-1}T^{-1}$

Here, B, P, and T denote the dimensions of plant biomass, pest density, and time, respectively.

2.2. Fundamental properties

The well-posedness of the proposed eco-epidemiological plant–pest model with dual transmission and allomone effects is established in this section. Since the right-hand side of System (2.1) is locally Lipschitz on bounded subsets of $\mathbb{R}^3_+$, the standard theory of ordinary differential equations guarantees the local existence and uniqueness of solutions for the associated initial value problem [45]. We also prove that the non-negative orthant is positively invariant and that all state variables remain bounded. These properties ensure that the local solution can be extended globally for all $t \geq 0$.

2.2.1. Existence and uniqueness

Theorem 1. *For every initial value $X_0 = (S_0, I_0, V_0) \in \mathbb{R}^3_+$, System (2.1) has a unique local solution $X(t) = (S(t), I(t), V(t))$ defined on a maximal interval $[0, T_{\max})$, where $0 < T_{\max} \leq \infty$.*

Proof. Let $\phi > 0$ and define

$$\Omega = \left\{X = (S, I, V) \in \mathbb{R}^3_+ :\ \|X\|_\infty \leq \phi\right\},$$

Let $X = (S, I, V)$, $\bar{X} = (\bar{S}, \bar{I}, \bar{V})$, and define the mapping $F(X) = (F_1(X), F_2(X), F_3(X))$, where

$$\begin{aligned} F_1(X) &= rS\left(1 - \frac{S+I}{K}\right) - (\beta_L I + \beta_T V)S - a_S S V, \\ F_2(X) &= (\beta_L I + \beta_T V)S - a_I I V - d_I I, \\ F_3(X) &= c_S S V + c_I I V - d_V V, \end{aligned} \tag{2.2}$$

For every $X, \bar{X} \in \Omega$, it holds that

$$\begin{aligned} \|F(X) - F(\bar{X})\| &= |F_1(X) - F_1(\bar{X})| + |F_2(X) - F_2(\bar{X})| + |F_3(X) - F_3(\bar{X})| \\ &\le r|S - \bar{S}| + \frac{r}{K}|S^2 - \bar{S}^2| + \frac{r}{K}|SI - \bar{S}\bar{I}| \\ &\quad + 2\beta_L|SI - \bar{S}\bar{I}| + 2\beta_T|SV - \bar{S}\bar{V}| + a_S|SV - \bar{S}\bar{V}| \\ &\quad + a_I|IV - \bar{I}\bar{V}| + d_I|I - \bar{I}| \\ &\quad + |c_S\|SV - \bar{S}\bar{V}| + |c_I\|IV - \bar{I}\bar{V}| + d_V|V - \bar{V}|, \end{aligned}$$

Since $X, \bar{X} \in \Omega$, all components of X and $\bar{X}$ are bounded above by ϕ. Thus,

$$\begin{aligned} |S^2 - \bar{S}^2| &\le 2\phi|S - \bar{S}|, \\ |SI - \bar{S}\bar{I}| &\le \phi|S - \bar{S}| + \phi|I - \bar{I}|, \\ |SV - \bar{S}\bar{V}| &\le \phi|S - \bar{S}| + \phi|V - \bar{V}|, \\ |IV - \bar{I}\bar{V}| &\le \phi|I - \bar{I}| + \phi|V - \bar{V}|, \end{aligned}$$

Substituting these inequalities into the previous estimate gives

$$\begin{aligned} \|F(X) - F(\bar{X})\| &\le \left(r + \frac{3\phi r}{K} + 2\beta_L\phi + 2\beta_T\phi + a_S\phi + |c_S|\phi\right)|S - \bar{S}| \\ &\quad + \left(\frac{\phi r}{K} + 2\beta_L\phi + a_I\phi + |c_I|\phi + d_I\right)|I - \bar{I}| \\ &\quad + (2\beta_T\phi + a_S\phi + a_I\phi + |c_S|\phi + |c_I|\phi + d_V)\,|V - \bar{V}| \\ &\le L_1|S - \bar{S}| + L_2|I - \bar{I}| + L_3|V - \bar{V}|, \end{aligned}$$

where

$$\begin{aligned} L_1 &= r + \frac{3\phi r}{K} + 2\beta_L\phi + 2\beta_T\phi + a_S\phi + |c_S|\phi, \\ L_2 &= \frac{\phi r}{K} + 2\beta_L\phi + a_I\phi + |c_I|\phi + d_I, \\ L_3 &= 2\beta_T\phi + a_S\phi + a_I\phi + |c_S|\phi + |c_I|\phi + d_V, \end{aligned}$$

Let $L = \max\{L_1, L_2, L_3\}$. Then

$$\|F(X) - F(\bar{X})\| \le L\left(|S - \bar{S}| + |I - \bar{I}| + |V - \bar{V}|\right) = L\|X - \bar{X}\|,$$

Therefore, F is locally Lipschitz on bounded subsets of $\mathbb{R}^3_+$. Hence, by the standard existence and uniqueness theorem for ordinary differential equations [45], for every $X_0 \in \mathbb{R}^3_+$, there is a unique local solution on a maximal interval $[0, T_{\max})$. □

2.2.2. Non-negativity

Theorem 2. *All solutions of System* (2.1) *with the initial condition* $X(0) = X_0 = (S_0, I_0, V_0) \in \mathbb{R}^3_+$ *are non-negative for all* $t \in [0, T_{\max})$.

Proof. We prove that all initial values $X(0) \in \mathbb{R}^3_+$ imply that the solution remains non-negative for every $t \in [0, T_{\max})$. First, consider $S(t)$. If $S_0 = 0$, then the susceptible plant biomass S remains on the boundary $S = 0$.

Next, assume that $S_0 > 0$. Suppose, by contradiction, that $S(t)$ can take negative values. Then $t_1 \in (0, T_{\max})$ exists such that

$$\begin{cases} S(t) > 0, & 0 < t < t_1, \\ S(t) = 0, & t = t_1, \\ S(t) < 0, & t > t_1, \end{cases}$$

Based on the first equation of System (2.1), the susceptible plant equation can be written as

$$\frac{dS}{dt} = S\left[r\left(1 - \frac{S+I}{K}\right) - \beta_L I - (\beta_T + a_S)V\right],$$

Hence, the boundary $S = 0$ is invariant. By uniqueness of solutions, a trajectory starting with $S_0 > 0$ cannot cross the invariant boundary $S = 0$. Therefore, $S(t) \geq 0$ for every $t \in [0, T_{\max})$.

Similarly, the pest equation can be written as

$$\frac{dV}{dt} = V(c_S S + c_I I - d_V),$$

Hence, the boundary $V = 0$ is invariant, and uniqueness implies that $V(t) \geq 0$ for every $t \in [0, T_{\max})$.

Next, consider $I(t)$. Assume that $I_0 > 0$. For contradiction, suppose that $I(t)$ becomes negative for some $t \in (0, T_{\max})$. Then $t_3 \in (0, T_{\max})$ exists such that

$$\begin{cases} I(t) > 0, & 0 < t < t_3, \\ I(t) = 0, & t = t_3, \\ I(t) < 0, & t > t_3, \end{cases}$$

Based on the second equation of System (2.1), at $t = t_3$, we obtain

$$\left.\frac{dI}{dt}\right|_{t=t_3} = \beta_T S(t_3) V(t_3),$$

Since $S(t_3) \geq 0$ and $V(t_3) \geq 0$, according to the previous arguments, it follows that $\left.\frac{dI}{dt}\right|_{t=t_3} \geq 0$. Thus, at the boundary $I = 0$, the vector field points inward or is tangent to the boundary. Consequently, the solution cannot leave $\mathbb{R}^3_+$ through the boundary $I = 0$, and hence $I(t) \geq 0$ for every $t \in [0, T_{\max})$. □

2.2.3. Boundedness

Lemma 1. *Let* $X(t)$ *be a non-negative solution of System (2.1) with the initial condition* $X(0) = X_0 \in \mathbb{R}^3_+$. *Then the total plant biomass* $S(t) + I(t)$ *is bounded. More precisely, if* $M = \max\{S_0 + I_0, K\}$, *then* $S(t) + I(t) \leq M$ *for all* $t \in [0, T_{\max})$. *Consequently,* $0 \leq S(t) \leq M$ *and* $0 \leq I(t) \leq M$ *for all* $t \in [0, T_{\max})$.

Proof. Define the total plant biomass as $N(t) = S(t) + I(t)$. Then $\frac{dN}{dt} = \frac{dS}{dt} + \frac{dI}{dt}$. Using the first and second equations of System (2.1), we obtain

$$\frac{dN}{dt} \leq rS\left(1 - \frac{N}{K}\right), \tag{2.3}$$

If $N(t) \geq K$, then $1 - \frac{N(t)}{K} \leq 0$. Because $S(t) \geq 0$, Inequality (2.3) implies $\frac{dN}{dt} \leq 0$. This means that whenever $N(t) \geq K$, the total plant biomass cannot increase. On the other hand, if $N(t) < K$, then $N(t)$ is already below K. It follows that $N(t)$ cannot exceed the larger value between its initial value and the carrying capacity. Thus, $N(t) \leq \max\{N(0), K\}$ for all $t \in [0, T_{\max})$. Substituting $N(0) = S_0 + I_0$ yields $S(t) + I(t) \leq M$, where $M = \max\{S_0 + I_0, K\}$. Because $S(t)$ and $I(t)$ are non-negative, $0 \leq S(t) \leq S(t) + I(t) \leq M$ and $0 \leq I(t) \leq S(t) + I(t) \leq M$. Accordingly, $0 \leq S(t) \leq M$ and $0 \leq I(t) \leq M$ for all $t \in [0, T_{\max})$. □

Lemma 2. *Assume that a positive constant θ exists such that $a_S - \theta c_S \geq 0$ and $a_I - \theta c_I \geq 0$. Then the pest density $V(t)$ is bounded for all $t \in [0, T_{\max})$.*

Proof. Define $W(t) = S(t) + I(t) + \theta V(t)$. Lemma 1 gives $S(t) + I(t) \leq M$ for all $t \in [0, T_{\max})$. Differentiating $W(t)$ along solutions of System (2.1) gives $\frac{dW}{dt} = \frac{dS}{dt} + \frac{dI}{dt} + \theta\frac{dV}{dt}$. Substituting System (2.1) leads to

$$\frac{dW}{dt} = rS\left(1 - \frac{S+I}{K}\right) - d_I I - (a_S - \theta c_S)SV - (a_I - \theta c_I)IV - \theta d_V V,$$

Under the stated assumption, the mixed terms satisfy $-(a_S - \theta c_S)SV \leq 0, -(a_I - \theta c_I)IV \leq 0$. As a result

$$\frac{dW}{dt} \leq rS\left(1 - \frac{S+I}{K}\right) - \theta d_V V, \tag{2.4}$$

Since $N(t) = S(t) + I(t) \geq S(t)$, we have $S\left(1 - \frac{N}{K}\right) = S\left(1 - \frac{S+I}{K}\right) \leq S\left(1 - \frac{S}{K}\right) \leq \frac{K}{4}$. Hence, $rS\left(1 - \frac{S+I}{K}\right) \leq \frac{rK}{4}$. Inequality (2.4) then gives $\frac{dW}{dt} \leq \frac{rK}{4} - \theta d_V V$. Equivalently, $\frac{dW}{dt} \leq \frac{rK}{4} - d_V W + d_V(S+I)$. Using Lemma 1, $S(t) + I(t) \leq M$, we obtain $\frac{dW}{dt} \leq \frac{rK}{4} + d_V M - d_V W$. By Gronwall's inequality [46], we obtain

$$W(t) \leq W(0)e^{-d_V t} + \left(\frac{rK}{4d_V} + M\right)(1 - e^{-d_V t}),$$

This estimate implies

$$W(t) \leq \max\left\{W(0), \frac{rK}{4d_V} + M\right\}$$

for all $t \in [0, T_{\max})$. Because $0 \leq \theta V(t) \leq W(t)$, we have

$$V(t) \leq \frac{1}{\theta}\max\left\{W(0), \frac{rK}{4d_V} + M\right\},$$

Thus, $V(t)$ remains bounded for all $t \in [0, T_{\max})$. □

Theorem 3. *Let $X(t)$ be a non-negative solution of System (2.1) with the initial condition $X(0) = X_0 \in \mathbb{R}^3_+$. If there is a positive constant θ satisfying $a_S - \theta c_S \geq 0, a_I - \theta c_I \geq 0$, then every non-negative solution of System (2.1) is bounded in $\mathbb{R}^3_+$ on $[0, T_{\max})$. More precisely, positive constants ρ_1, ρ_2, ρ_3 exist such that $S(t) \leq \rho_1, I(t) \leq \rho_2$, and $V(t) \leq \rho_3$ for all $t \in [0, T_{\max})$.*

Proof. From Lemma 1, the total plant biomass satisfies $S(t) + I(t) \leq M$ for all $t \in [0, T_{\max})$. Since $S(t)$ and $I(t)$ are non-negative, we have $0 \leq S(t) \leq M$ and $0 \leq I(t) \leq M$. Accordingly, one may choose $\rho_1 = \rho_2 = M$. Furthermore, by Lemma 2, the pest density $V(t)$ is bounded. This gives a positive constant ρ_3 such that $V(t) \leq \rho_3$ for all $t \in [0, T_{\max})$. It follows that every non-negative solution of System (2.1) remains in a bounded subset of $\mathbb{R}^3_+$ on $[0, T_{\max})$. □

Remark 1. *Since $a_S > 0$ and $a_I > 0$, a sufficiently small positive constant θ can always be chosen such that*

$$a_S - \theta c_S \geq 0, \qquad a_I - \theta c_I \geq 0,$$

Therefore, the conditions of Theorem 3 can always be satisfied for a sufficiently small positive θ.

Corollary 1. *For every initial condition $X_0 \in \mathbb{R}^3_+$, the solution of System* (2.1) *exists uniquely for all $t \geq 0$.*

Proof. By Theorem 1, System (2.1) admits a unique local solution on a maximal interval $[0, T_{\max})$. The positive invariance of $\mathbb{R}^3_+$ ensures that the solution remains non-negative, while Theorem 3 shows that the solution remains in a bounded subset of $\mathbb{R}^3_+$ on $[0, T_{\max})$. Therefore, finite-time blow-up cannot occur. By the continuation theorem for ordinary differential equations, $T_{\max} = \infty$. Hence, the solution exists uniquely for all $t \geq 0$. □

3. Analytical results

3.1. Equilibria and invasion thresholds

3.1.1. Equilibria

System (2.1) admits the following equilibrium types.

(a) The population-free equilibrium point $E_0 = (0, 0, 0)$, which always exists.
(b) The susceptible plant-only equilibrium point $E_1 = (K, 0, 0)$, which also always exists.
(c) The pest-free infected equilibrium point $E_2 = (S_2, I_2, 0)$, where $S_2 = \frac{d_I}{\beta_L}$ and $I_2 = \frac{r(K\beta_L - d_I)}{\beta_L(r + K\beta_L)}$. The equilibrium E_2 is feasible if $K\beta_L > d_I$.
(d) The coexistence equilibrium is denoted $E_3 = (S^*, I^*, V^*)$, where $S^* > 0$, $I^* > 0$, and $V^* > 0$. From the third equilibrium equation, we obtain $c_S S^* + c_I I^* = d_V$. For $c_I \neq 0$, this gives

$$I^* = \frac{d_V - c_S S^*}{c_I},$$

Substituting this expression into the second equilibrium equation yields

$$V^* = \frac{(\beta_L S^* - d_I)(d_V - c_S S^*)}{a_I(d_V - c_S S^*) - c_I \beta_T S^*},$$

provided that $a_I(d_V - c_S S^*) - c_I \beta_T S^* \neq 0$. Substituting these expressions into the first equilibrium equation gives

$$D_0 (S^*)^2 + D_1 S^* + D_2 = 0, \tag{3.1}$$

where

$$D_0 = -P_1Q_1 + (\beta_T + a_S)\beta_L c_S,$$
$$D_1 = P_1Q_0 - P_0Q_1 - (\beta_T + a_S)(\beta_L d_V + c_S d_I),$$
$$D_2 = P_0Q_0 + (\beta_T + a_S)d_I d_V,$$

with

$$P_0 = r - \frac{\left(\frac{r}{K} + \beta_L\right)d_V}{c_I}, \qquad P_1 = -\frac{r}{K} + \frac{\left(\frac{r}{K} + \beta_L\right)c_S}{c_I},$$
$$Q_0 = a_I d_V, \qquad Q_1 = a_I c_S + c_I\beta_T,$$

For $D_0 \neq 0$, the roots of Equation (3.1) are

$$S^*_{1,2} = \frac{-D_1 \pm \sqrt{\Delta}}{2D_0}, \qquad \Delta = D_1^2 - 4D_0D_2,$$

If $\Delta < 0$, no real roots exist. If $\Delta = 0$, the repeated root $S^* = -D_1/(2D_0)$ is positive if and only if $D_0D_1 < 0$.
For $\Delta > 0$, the signs of the two distinct roots are classified as follows.

(a) If $D_2 > 0$, two cases arise.

i. When $D_0 < 0$, we have $\sqrt{\Delta} > |D_1|$. Since $2D_0 < 0$, it follows that

$$S^*_1 < 0, \qquad S^*_2 > 0,$$

ii. When $D_0 > 0$, we have $\sqrt{\Delta} < |D_1|$. Consequently,

$$\begin{cases} S^*_1 > 0, & S^*_2 > 0, \quad D_1 < 0, \\ S^*_1 < 0, & S^*_2 < 0, \quad D_1 > 0, \end{cases}$$

(b) If $D_2 < 0$, the corresponding cases are.

i. When $D_0 > 0$, we have $\sqrt{\Delta} > |D_1|$, yielding

$$S^*_1 > 0, \qquad S^*_2 < 0,$$

ii. When $D_0 < 0$, we have $\sqrt{\Delta} < |D_1|$. Hence,

$$\begin{cases} S^*_1 > 0, & S^*_2 > 0, \quad D_1 > 0, \\ S^*_1 < 0, & S^*_2 < 0, \quad D_1 < 0, \end{cases}$$

If $D_2 = 0$, one root is zero, whereas the other root $-D_1/D_0$ is positive if and only if $D_0D_1 < 0$. However, a positive root S^* does not necessarily yield a biologically feasible coexistence equilibrium. Each positive root must also satisfy

$$\frac{d_V - c_S S^*}{c_I} > 0, \qquad \frac{(\beta_L S^* - d_I)(d_V - c_S S^*)}{a_I(d_V - c_S S^*) - c_I\beta_T S^*} > 0,$$

with a nonzero denominator. In particular, when $c_S > 0$ and $c_I > 0$, the positivity condition for I^* reduces to

$$0 < S^* < \frac{d_V}{c_S},$$

Therefore, although Equation (3.1) may admit two positive roots, only those satisfying the above feasibility conditions correspond to biologically admissible coexistence equilibria.

The preceding reduction assumes $c_I \neq 0$ and a nonzero denominator in the expression for V^*. If $c_I = 0$, the third equilibrium equation reduces to $c_S S^* = d_V$, while a vanishing denominator requires a direct examination of the original equilibrium equations. Similarly, if $D_0 = 0$ and $D_1 \neq 0$, Equation (3.1) becomes linear, with $S^* = -D_2/D_1$. The degenerate case $D_0 = D_1 = 0$ must be examined separately using the original equilibrium equations.

3.1.2. Direct transmission and pest density invasion thresholds

The proposed model includes two coupled modes of invasion: One associated with the growth of infected plant biomass through direct plant-to-plant transmission on the pest-free subspace, and the other associated with pest density invading pest-free boundary states. Such threshold-based formulations are extensively used in plant disease and vector-borne plant virus models to characterize infections' persistence, pest density invasion, and disease control outcomes [36, 47–51]. Therefore, early invasion dynamics cannot be adequately characterized by a single threshold value.

The relevant pest-free boundary equilibria are $E_1 = (K, 0, 0)$ and $E_2 = (S_2, I_2, 0)$, where E_2 exists if $K\beta_L > d_I$.

Proposition 4. *On the pest-free invariant subspace $V = 0$, the direct transmission invasion threshold around the susceptible plant-only equilibrium $E_1 = (K, 0, 0)$ is given by $\mathcal{R}_I = \frac{\beta_L K}{d_I}$. Hence, infected plant biomass can invade E_1 through direct plant-to-plant transmission if and only if $\mathcal{R}_I > 1$.*

Proof. To determine the direct transmission invasion threshold, we restrict the system to the pest-free invariant subspace $V = 0$. In this subspace, the infected plant equation becomes

$$\frac{dI}{dt} = \beta_L S I - d_I I,$$

Around the susceptible plant-only equilibrium $E_1 = (K, 0, 0)$, linearization gives

$$\frac{dI}{dt} = (\beta_L K - d_I) I,$$

Therefore, a small infected-plant perturbation can increase through direct plant-to-plant transmission if $\beta_L K - d_I > 0$. This condition is equivalent to

$$\frac{\beta_L K}{d_I} > 1,$$

Hence, the direct transmission invasion threshold is

$$\mathcal{R}_I = \frac{\beta_L K}{d_I},$$

Consequently, infected plant biomass can invade E_1 through direct plant-to-plant transmission if and only if $\mathcal{R}_I > 1$. □

Proposition 5. *The pest density invasion threshold around the susceptible plant-only equilibrium* $E_1 = (K, 0, 0)$ *is* $\mathcal{R}_V^{(1)} = \dfrac{c_S K}{d_V}$. *Moreover, if* $E_2 = (S_2, I_2, 0)$ *exists, then the pest density invasion threshold around* E_2 *is* $\mathcal{R}_V^{(2)} = \frac{c_S S_2 + c_I I_2}{d_V} = \frac{1}{d_V}\left[\frac{c_S d_I}{\beta_L} + \frac{c_I r(K\beta_L - d_I)}{\beta_L(r + K\beta_L)}\right]$. *Hence, pest density can invade* E_1 *if and only if* $\mathcal{R}_V^{(1)} > 1$, *and it can invade* E_2 *if and only if* $\mathcal{R}_V^{(2)} > 1$.

Proof. The pest density equation of System (2.1) is $\frac{dV}{dt} = c_S S V + c_I I V - d_V V$. Factoring out V, we obtain $\frac{dV}{dt} = (c_S S + c_I I - d_V)V$. Thus, the per capita growth rate of pest density is $c_S S + c_I I - d_V$.

First, we evaluate this quantity at the susceptible plant-only equilibrium $E_1 = (K, 0, 0)$. Since $S = K$ and $I = 0$, we have $c_S S + c_I I - d_V = c_S K - d_V$. Therefore, near E_1, the linearized pest density equation is

$$\frac{dV}{dt} = (c_S K - d_V)V,$$

Pest density can increase from a small initial value if $c_S K - d_V > 0$. This is equivalent to $\frac{c_S K}{d_V} > 1$. Hence,

$$\mathcal{R}_V^{(1)} = \frac{c_S K}{d_V},$$

Next, assume that $E_2 = (S_2, I_2, 0)$ exists. Evaluating the pest density per capita growth rate at E_2, we obtain $c_S S_2 + c_I I_2 - d_V$. Thus, near E_2, the linearized pest density equation is

$$\frac{dV}{dt} = (c_S S_2 + c_I I_2 - d_V)V,$$

Pest density can invade E_2 if $c_S S_2 + c_I I_2 - d_V > 0$. Equivalently, $\frac{c_S S_2 + c_I I_2}{d_V} > 1$. Therefore, we have

$$\mathcal{R}_V^{(2)} = \frac{c_S S_2 + c_I I_2}{d_V},$$

Substituting $S_2 = \frac{d_I}{\beta_L}$ and $I_2 = \frac{r(K\beta_L - d_I)}{\beta_L(r + K\beta_L)}$, we obtain

$$\mathcal{R}_V^{(2)} = \frac{1}{d_V}\left[\frac{c_S d_I}{\beta_L} + \frac{c_I r(K\beta_L - d_I)}{\beta_L(r + K\beta_L)}\right],$$

Hence, pest density can invade E_2 if and only if $\mathcal{R}_V^{(2)} > 1$. □

Remark 2. *The threshold* $\mathcal{R}_I$ *characterizes direct plant-to-plant transmission on the pest-free invariant subspace* $V = 0$ *and should not be interpreted as a general infection reproduction number for the full three-dimensional system. Indeed, the linearized* (I, V) *dynamics around* $E_1 = (K, 0, 0)$ *are governed by*

$$\begin{pmatrix} \dot{I} \\ \dot{V} \end{pmatrix} = \begin{pmatrix} \beta_L K - d_I & \beta_T K \\ 0 & c_S K - d_V \end{pmatrix} \begin{pmatrix} I \\ V \end{pmatrix},$$

Hence, the two invasion eigenvalues are $\lambda_I = \beta_L K - d_I$ *and* $\lambda_V = c_S K - d_V$. *Although* β_T *does not alter these eigenvalues because the linearized matrix is upper triangular, it couples pest invasion to infected plant production through the term* $\beta_T K V$. *Consequently, when* $\mathcal{R}_I < 1$ *but* $\mathcal{R}_V^{(1)} > 1$, *direct transmission alone is subcritical, whereas pest invasion can still generate infected plant biomass through effective vector-mediated transmission. Thus,* $\mathcal{R}_I$ *and* $\mathcal{R}_V^{(1)}$ *describe distinct but coupled invasion mechanisms.*

Remark 3. *The limiting cases of the two transmission pathways provide further biological interpretation. If $\beta_T = 0$, infection is transmitted only through direct plant-to-plant contact. In the pest-free subsystem $V = 0$, the infected plant equation reduces to*

$$\frac{dI}{dt} = I(\beta_L S - d_I),$$

so that direct transmission alone can support infection invasion when $\mathcal{R}_I = \beta_L K/d_I > 1$.

If $\beta_L = 0$, infection is generated only through the vector-mediated pathway, and

$$\frac{dI}{dt} = \beta_T VS - a_I IV - d_I I,$$

Thus, under the effective-transmission interpretation adopted here, persistent pest density can generate infected plant biomass through $\beta_T VS$ and may sustain infection without direct plant-to-plant transmission if the resulting infection input is sufficient to balance infected biomass losses. This conclusion depends on the assumed effective infectious fraction of the pest population; an explicit pathogen acquisition mechanism would require separate non-infectious and infectious pest classes.

Remark 4. *The allomone parameters affect not only the equilibrium densities but also the pest-invasion boundaries. Since $c_S = \gamma_S a_S - \eta_S$, the condition $\mathcal{R}_V^{(1)} = 1$ gives the critical boundary*

$$d_V^{\text{crit},1} = c_S K = (\gamma_S a_S - \eta_S)K,$$

Hence, we have

$$\frac{\partial d_V^{\text{crit},1}}{\partial \eta_S} = -K < 0,$$

Thus, increasing the allomone-mediated reduction η_S shifts the pest invasion boundary toward lower values of d_V, thereby making pest invasion of the susceptible plant-only equilibrium more difficult.

Similarly, the pest invasion boundary at the pest-free infected equilibrium $E_2 = (S_2, I_2, 0)$ is determined by $\mathcal{R}_V^{(2)} = 1$, or, equivalently,

$$d_V^{\text{crit},2} = c_S S_2 + c_I I_2 = (\gamma_S a_S - \eta_S)S_2 + (\gamma_I a_I - \eta_I)I_2,$$

Since S_2 and I_2 are determined on the pest-free invariant subspace and therefore do not depend on η_S or η_I, we have

$$\frac{\partial d_V^{\text{crit},2}}{\partial \eta_S} = -S_2 < 0, \qquad \frac{\partial d_V^{\text{crit},2}}{\partial \eta_I} = -I_2 < 0,$$

Consequently, stronger allomone effects associated with either susceptible or infected plant biomass reduce the pest growth threshold and shift the corresponding invasion boundary. Therefore, the allomone parameters modify the qualitative transition between pest-free and pest-persistent regimes, rather than merely changing the densities of the coexistence equilibrium.

3.2. Local stability analysis

Here, we analyze the local stability of equilibria of System (2.1). We linearize System (2.1) and write the Jacobian matrix at any equilibrium point $E_i(S, I, V)$, $i = 0, 1, 2, 3$, as follows:

$$J(E_i) = \begin{pmatrix} j_{11} & j_{12} & j_{13} \\ j_{21} & j_{22} & j_{23} \\ j_{31} & j_{32} & j_{33} \end{pmatrix}, \tag{3.14}$$

where

$$\begin{aligned} j_{11} &= r - \frac{2rS}{K} - \frac{rI}{K} - \beta_L I - (\beta_T + a_S)V, \qquad j_{12} = -\frac{rS}{K} - \beta_L S, \\ j_{13} &= -(\beta_T + a_S)S, \qquad j_{21} = \beta_L I + \beta_T V, \qquad j_{22} = \beta_L S - a_I V - d_I, \\ j_{23} &= \beta_T S - a_I I, \qquad j_{31} = c_S V, \qquad j_{32} = c_I V, \qquad j_{33} = c_S S + c_I I - d_V, \end{aligned}$$

At the population-free equilibrium $E_0 = (0, 0, 0)$, the Jacobian matrix becomes

$$J(E_0) = \begin{pmatrix} r & 0 & 0 \\ 0 & -d_I & 0 \\ 0 & 0 & -d_V \end{pmatrix},$$

The eigenvalues of $J(E_0)$ are $\lambda_1 = r$, $\lambda_2 = -d_I$, and $\lambda_3 = -d_V$. Since $r > 0$, one eigenvalue is positive. Therefore, E_0 is always unstable.

At the susceptible plant-only equilibrium $E_1 = (K, 0, 0)$, we obtain

$$J(E_1) = \begin{pmatrix} -r & -r - \beta_L K & -(\beta_T + a_S)K \\ 0 & \beta_L K - d_I & \beta_T K \\ 0 & 0 & c_S K - d_V \end{pmatrix},$$

Since $J(E_1)$ is an upper triangular matrix, its eigenvalues are $\lambda_1 = -r$, $\lambda_2 = \beta_L K - d_I$, and $\lambda_3 = c_S K - d_V$. Therefore, E_1 is locally asymptotically stable if $\beta_L K < d_I$ and $c_S K < d_V$. Equivalently, $\mathcal{R}_I < 1$ and $\mathcal{R}_V^{(1)} < 1$.

Here, λ_2 corresponds to the direct transmission invasion direction on the pest-free invariant subspace $V = 0$, whereas λ_3 corresponds to the pest density invasion direction. Although the effective vector-mediated transmission coefficient β_T does not appear explicitly in these eigenvalues, it enters the off-diagonal term $\beta_T K$ and couples pest perturbations to the infected plant component. Thus, local asymptotic stability of E_1 in the full three-dimensional system requires both invasion eigenvalues to be negative.

Now consider the pest-free infected equilibrium $E_2 = (S_2, I_2, 0)$. At E_2, the Jacobian matrix takes the block triangular form

$$J(E_2) = \begin{pmatrix} a_{11} & a_{12} & a_{13} \\ a_{21} & a_{22} & a_{23} \\ 0 & 0 & a_{33} \end{pmatrix},$$

where

$$a_{11} = r\left(1 - \frac{2S_2 + I_2}{K}\right) - \beta_L I_2, \qquad a_{12} = -\frac{rS_2}{K} - \beta_L S_2, \qquad a_{13} = -(\beta_T + a_S)S_2,$$

$$a_{21} = \beta_L I_2, \qquad a_{22} = \beta_L S_2 - d_I, \qquad a_{23} = \beta_T S_2 - a_I I_2, \qquad a_{33} = c_S S_2 + c_I I_2 - d_V,$$

Since $S_2 = \frac{d_I}{\beta_L}$, we obtain $a_{22} = 0$. Moreover, using the equilibrium relation $r\left(1 - \frac{S_2+I_2}{K}\right) - \beta_L I_2 = 0$, we have $a_{11} = r\left(1 - \frac{2S_2+I_2}{K}\right) - \beta_L I_2 = -\frac{rS_2}{K} < 0$.

The characteristic equation of $J(E_2)$ is given by $\det(J(E_2) - \lambda I) = 0$. Since $J(E_2)$ is block triangular, one eigenvalue is $\lambda_1 = a_{33} = c_S S_2 + c_I I_2 - d_V$. The remaining two eigenvalues are obtained from $\lambda^2 - a_{11}\lambda - a_{12}a_{21} = 0$.

For this two-dimensional block, the trace and determinant are

$$\text{tr} = a_{11} < 0 \quad \text{and} \quad \det = -a_{12}a_{21} > 0,$$

because $a_{12} < 0$ and $a_{21} > 0$ whenever E_2 exists. Hence, the two eigenvalues associated with the (S, I)-subsystem have negative real parts.

Thus, the local stability of E_2 is determined by the sign of a_{33}. Since $a_{33} = c_S S_2 + c_I I_2 - d_V$, we have $a_{33} < 0$ if and only if $c_S S_2 + c_I I_2 < d_V$. Equivalently, $\mathcal{R}_V^{(2)} < 1$. Therefore, the pest-free infected equilibrium E_2 is locally asymptotically stable if $\mathcal{R}_V^{(2)} < 1$. If $\mathcal{R}_V^{(2)} > 1$, then $a_{33} > 0$, and pest density can invade E_2. Consequently, E_2 becomes unstable.

Now consider the coexistence equilibrium $E_3 = (S^*, I^*, V^*)$, where $S^* > 0$, $I^* > 0$, and $V^* > 0$. The Jacobian matrix at E_3 can be written as

$$J(E_3) = \begin{pmatrix} b_{11} & b_{12} & b_{13} \\ b_{21} & b_{22} & b_{23} \\ b_{31} & b_{32} & 0 \end{pmatrix}, \tag{3.15}$$

where

$$\begin{aligned} b_{11} &= -\frac{rS^*}{K}, & b_{12} &= -\frac{rS^*}{K} - \beta_L S^*, & b_{13} &= -(\beta_T + a_S)S^*, \\ b_{21} &= \beta_L I^* + \beta_T V^*, & b_{22} &= \beta_L S^* - a_I V^* - d_I, & b_{23} &= \beta_T S^* - a_I I^*, \\ b_{31} &= c_S V^*, & b_{32} &= c_I V^*, \end{aligned}$$

The characteristic equation of $J(E_3)$ can be written as

$$\lambda^3 + K_1\lambda^2 + K_2\lambda + K_3 = 0, \tag{3.16}$$

where

$$\begin{aligned} K_1 &= -(b_{11} + b_{22}), \\ K_2 &= b_{11}b_{22} - b_{12}b_{21} - b_{13}b_{31} - b_{23}b_{32}, \\ K_3 &= b_{32}b_{11}b_{23} - b_{31}b_{12}b_{23} - b_{32}b_{13}b_{21} + b_{31}b_{13}b_{22}, \end{aligned}$$

By the Routh–Hurwitz criterion [52], the coexistence equilibrium E_3 is locally asymptotically stable if $K_1 > 0$, $K_3 > 0$, and $K_1K_2 > K_3$, provided that S^* is a positive real root of Equation (3.1) satisfying the biological feasibility conditions $I^* > 0$ and $V^* > 0$.

3.3. Persistence

Long-term coexistence is an important property in systems involving interacting biological populations. For System (2.1), this requires showing that susceptible plant biomass, infected plant biomass, and pest density remain uniformly away from extinction. In this section, uniform persistence is established by using the Butler–McGehee lemma together with the persistence framework of [53].

Proposition 6. *Suppose that $\beta_T > 0$ and the threshold quantities satisfy $\mathcal{R}_I > 1$, $\mathcal{R}_V^{(1)} > 1$, and $\mathcal{R}_V^{(2)} > 1$. Then System (2.1) is uniformly persistent. More precisely, the positive constants $m_1, m_2, m_3 > 0$ exist such that all solutions of System (2.1) with the initial condition $X(0) = X_0 \in \text{int}(\mathbb{R}^3_+)$ satisfy*

$$\liminf_{t\to\infty} S(t) \geq m_1, \qquad \liminf_{t\to\infty} I(t) \geq m_2, \qquad \liminf_{t\to\infty} V(t) \geq m_3,$$

Proof. By Theorem 2, $\mathbb{R}^3_+$ is positively invariant under System (2.1). Moreover, by Theorem 3, all positive solutions of System (2.1) are bounded. Hence, for every initial condition $X(0) = X_0 \in \text{int}(\mathbb{R}^3_+)$, the positive orbit $O^+(X_0)$ is precompact and has a non-empty compact omega-limit set $\omega(X_0)$. It remains to show that $\omega(X_0)$ cannot intersect the boundary $\partial\mathbb{R}^3_+ = \{(S, I, V) \in \mathbb{R}^3_+ : SIV = 0\}$.

First, observe that the plane $I = 0$ is not invariant whenever $S > 0$ and $V > 0$, since

$$\left.\frac{dI}{dt}\right|_{I=0} = \beta_T S V > 0,$$

Thus, the relevant invariant boundary dynamics are contained in the planes $S = 0$ and $V = 0$.

On the plane $S = 0$, System (2.1) reduces to $\frac{dI}{dt} = -(a_I V + d_I)I$ and $\frac{dV}{dt} = (c_I I - d_V)V$. Since $\frac{dI}{dt} \leq -d_I I$, we have $I(t) \to 0$ as $t \to \infty$. Consequently, $V(t) \to 0$. Hence, every orbit on $S = 0$ approaches $E_0 = (0, 0, 0)$.

On the plane $V = 0$, the boundary subsystem becomes

$$\begin{aligned} \frac{dS}{dt} &= rS\left(1 - \frac{S + I}{K}\right) - \beta_L S I, \\ \frac{dI}{dt} &= \beta_L S I - d_I I, \end{aligned}$$

The equilibria of this subsystem are $E_0 = (0, 0, 0)$, $E_1 = (K, 0, 0)$, and, when $\mathcal{R}_I > 1$, $E_2 = (S_2, I_2, 0)$. Furthermore, using the Dulac function $B(S, I) = \frac{1}{SI}$, we obtain

$$\frac{\partial}{\partial S}\left(B\frac{dS}{dt}\right) + \frac{\partial}{\partial I}\left(B\frac{dI}{dt}\right) = -\frac{r}{KI} < 0$$

for $S > 0$ and $I > 0$. Therefore, by the Bendixson–Dulac criterion, there is no periodic orbit in the interior of the $S - I$ boundary plane.

Let $\mathcal{M}_\partial$ denote the maximal invariant set of System (2.1) contained in $\partial\mathbb{R}^3_+$. Since the portion of the plane $I = 0$ with $S > 0$ and $V > 0$ is not invariant, the preceding analysis shows that $\mathcal{M}_\partial$ is generated by the boundary equilibria E_0, E_1, and E_2, together with the connecting orbits between them.

At E_0, the eigenvalue in the S-direction is $r > 0$. Consequently, E_0 is unstable. The positive unstable branch of E_0 on the S-axis approaches E_1. Therefore, by the Butler–McGehee lemma, if $E_0 \in \omega(X_0)$ for a positive interior orbit, then $E_1 \in \omega(X_0)$.

At E_1, the invasion eigenvalues are $\beta_L K - d_I$ and $c_S K - d_V$. Since $\mathcal{R}_I > 1$ and $\mathcal{R}_V^{(1)} > 1$, both eigenvalues are positive. Hence, E_1 is repelling with respect to direct transmission invasion and pest density invasion. Moreover, on the invariant plane $V = 0$, the boundary dynamics lead from E_1 to E_2. Thus, again by the Butler–McGehee argument, if $E_1 \in \omega(X_0)$, then $E_2 \in \omega(X_0)$.

Finally, at E_2, the transversal eigenvalue in the V-direction is $c_S S_2 + c_I I_2 - d_V$. Since $\mathcal{R}_V^{(2)} > 1$, this eigenvalue is positive. Therefore, there is a neighborhood of E_2 in which $c_S S + c_I I - d_V > 0$. Hence, any solution with $V > 0$ being sufficiently close to E_2 satisfies $\dot{V} > 0$ and cannot converge to E_2. Consequently, the stable set of E_2 does not intersect $\text{int}(\mathbb{R}^3_+)$.

Consequently, the boundary invariant structure is acyclic, with the boundary equilibria ordered through

$$E_0 \to E_1 \to E_2,$$

and the stable sets of the boundary invariant components do not intersect $\text{int}(\mathbb{R}^3_+)$ under the stated threshold conditions. Since all positive orbits are precompact, the standard persistence theorem of Freedman and Waltman [53] implies that System (2.1) is uniformly persistent. Therefore, the constants $m_1, m_2, m_3 > 0$ exist such that

$$\liminf_{t\to\infty} S(t) \geq m_1, \qquad \liminf_{t\to\infty} I(t) \geq m_2, \qquad \liminf_{t\to\infty} V(t) \geq m_3,$$

□

3.4. Global stability analysis

We now investigate the global stability of the coexistence equilibrium $E_3 = (S^*, I^*, V^*)$ of System (2.1) by applying the high-dimensional Bendixson criterion. Since System (2.1) is three-dimensional, the second additive compound matrix associated with the Jacobian matrix is of order 3×3. The main objective is to establish that the corresponding second compound system is equi-uniformly asymptotically stable along all positive solutions. This approach follows the geometric criterion of Li and Muldowney [54, 55].

Let $X = (S, I, V)^T$ and $F(X) = (F_1, F_2, F_3)^T$ be as defined in (2.2). Then System (2.1) can be written as

$$\frac{dX}{dt} = F(X), \tag{3.17}$$

The Jacobian matrix of System (2.1) follows from Matrix (3.14).

For a three-dimensional system, the second additive compound matrix of J is

$$J^{[2]} = \begin{pmatrix} j_{11} + j_{22} & j_{23} & -j_{13} \\ j_{32} & j_{11} + j_{33} & j_{12} \\ -j_{31} & j_{21} & j_{22} + j_{33} \end{pmatrix} = \begin{pmatrix} \ell_{11} & \ell_{12} & \ell_{13} \\ \ell_{21} & \ell_{22} & \ell_{23} \\ \ell_{31} & \ell_{32} & \ell_{33} \end{pmatrix}, \tag{3.18}$$

where

$$\ell_{11} = r - d_I - \frac{2rS}{K} - \frac{rI}{K} - \beta_L I + \beta_L S - (\beta_T + a_S + a_I)V,$$

$$\ell_{12} = \beta_T S - a_I I, \qquad \ell_{13} = (\beta_T + a_S)S, \qquad \ell_{21} = c_I V, \qquad \ell_{23} = -\frac{rS}{K} - \beta_L S,$$

$$\ell_{22} = r - d_V - \frac{2rS}{K} - \frac{rI}{K} - \beta_L I - (\beta_T + a_S)V + c_S S + c_I I,$$
$$\ell_{31} = -c_S V, \qquad \ell_{32} = \beta_L I + \beta_T V, \qquad \ell_{33} = \beta_L S - a_I V - d_I + c_S S + c_I I - d_V,$$

Thus, the second compound system associated with System (2.1) is

$$\frac{dZ}{dt} = J^{[2]}(S(t), I(t), V(t))Z, \qquad Z = (z_1, z_2, z_3)^T, \tag{3.19}$$

where

$$\dot{z}_1 = \ell_{11}z_1 + \ell_{12}z_2 + \ell_{13}z_3,$$
$$\dot{z}_2 = \ell_{21}z_1 + \ell_{22}z_2 + \ell_{23}z_3,$$
$$\dot{z}_3 = \ell_{31}z_1 + \ell_{32}z_2 + \ell_{33}z_3,$$

Here, $X(t) = (S(t), I(t), V(t))^T$ is an arbitrary solution of System (2.1) with $X(0) = X_0 = (S_0, I_0, V_0) \in \mathbb{R}^3_+$.

A suitable Lyapunov function is required to show the uniform asymptotic stability of the set of linear equations (3.19). For further illustration, we consider a positive definite function $\Xi(Z)$, which is independent of initial points, such that $D^+\Xi(Z)$ is negative definite and also independent of the initial points.

For a detailed analysis of the global stability of System (2.1) using Li and Muldowney's high-dimensional Bendixson criterion [54], we use the proposition as in Proposition 4.1 of Sun and Loreau [38]. By Theorem 3 and Proposition 6, the boundedness and uniform persistence of System (2.1) ensure the existence of the positive constants m_i and ρ_i, $i = 1, 2, 3$, independent of the positive initial conditions, such that

$$m_1 \le S(t) \le \rho_1, \qquad m_2 \le I(t) \le \rho_2, \qquad m_3 \le V(t) \le \rho_3 \tag{3.20}$$

for all sufficiently large values of t, where the entry time may depend on the initial condition. These bounds are used to estimate the coefficients of the second additive compound system. We now introduce the following assumption.

Assumption (H). The positive constants δ_2, δ_3, and Ψ exist such that

$$\max\left\{p_{11} + \frac{q_{12}}{\delta_2} + \frac{q_{13}}{\delta_3},\ \delta_2 q_{21} + p_{22} + \frac{\delta_2}{\delta_3}q_{23},\ \delta_3 q_{31} + \frac{\delta_3}{\delta_2}q_{32} + p_{33}\right\} \le -\Psi < 0, \tag{3.21}$$

Now, we form

$$\Xi(Z) = \max\{|z_1|, \delta_2|z_2|, \delta_3|z_3|\}, \tag{3.22}$$

where $\delta_2 > 0$ and $\delta_3 > 0$.

Direct calculations yield the following inequalities:

$$D^+|z_1| \le p_{11}|z_1| + q_{12}|z_2| + q_{13}|z_3|,$$
$$D^+(\delta_2|z_2|) \le \delta_2\left(q_{21}|z_1| + p_{22}|z_2| + q_{23}|z_3|\right),$$
$$D^+(\delta_3|z_3|) \le \delta_3\left(q_{31}|z_1| + q_{32}|z_2| + p_{33}|z_3|\right),$$

Using the uniform bounds in (3.20), the coefficients in the estimates above are given by

$$
\begin{aligned}
p_{11} &= r - d_I - \frac{2rm_1}{K} - \frac{rm_2}{K} - \beta_L m_2 + \beta_L \rho_1 - (\beta_T + a_S + a_I)m_3,\\
p_{22} &= r - d_V - \frac{2rm_1}{K} - \frac{rm_2}{K} - \beta_L m_2 - (\beta_T + a_S)m_3 + c_S^+ \rho_1 + c_S^- m_1 + c_I^+ \rho_2 + c_I^- m_2,\\
p_{33} &= \beta_L \rho_1 + c_S^+ \rho_1 + c_S^- m_1 + c_I^+ \rho_2 + c_I^- m_2 - a_I m_3 - d_I - d_V,\\
q_{12} &= \max_{\substack{m_1 \le S \le \rho_1 \\ m_2 \le I \le \rho_2}} |\beta_T S - a_I I|, \qquad q_{13} = (\beta_T + a_S)\rho_1, \qquad q_{21} = |c_I|\rho_3,\\
q_{23} &= \left(\frac{r}{K} + \beta_L\right)\rho_1, \qquad q_{31} = |c_S|\rho_3, \qquad q_{32} = \beta_L \rho_2 + \beta_T \rho_3,
\end{aligned}
$$

Here, $c_S^+ = \max\{c_S, 0\}$, $c_S^- = \min\{c_S, 0\}$, $c_I^+ = \max\{c_I, 0\}$, and $c_I^- = \min\{c_I, 0\}$. These expressions account for all possible signs of c_S and c_I.

Let

$$
\mathcal{I}(t) = \{i \in \{1, 2, 3\} : \delta_i |z_i(t)| = \Xi(Z(t))\}, \qquad \delta_1 = 1,
$$

For each active index $i \in \mathcal{I}(t)$, the corresponding weighted component equals $\Xi(Z(t))$. Consequently, we have

$$
\begin{aligned}
D^+|z_1| &\le \left(p_{11} + \frac{q_{12}}{\delta_2} + \frac{q_{13}}{\delta_3}\right)\Xi(Z), && \text{if } 1 \in \mathcal{I}(t),\\
D^+(\delta_2|z_2|) &\le \left(\delta_2 q_{21} + p_{22} + \frac{\delta_2}{\delta_3} q_{23}\right)\Xi(Z), && \text{if } 2 \in \mathcal{I}(t),\\
D^+(\delta_3|z_3|) &\le \left(\delta_3 q_{31} + \frac{\delta_3}{\delta_2} q_{32} + p_{33}\right)\Xi(Z), && \text{if } 3 \in \mathcal{I}(t),
\end{aligned}
$$

Since the upper right Dini derivative of a finite maximum is controlled by its active components, we obtain

$$
D^+\Xi(Z(t)) \le \omega\, \Xi(Z(t)), \tag{3.23}
$$

where

$$
\omega = \max\left\{p_{11} + \frac{q_{12}}{\delta_2} + \frac{q_{13}}{\delta_3},\ \delta_2 q_{21} + p_{22} + \frac{\delta_2}{\delta_3} q_{23},\ \delta_3 q_{31} + \frac{\delta_3}{\delta_2} q_{32} + p_{33}\right\},
$$

By Assumption *(H)*, $\Psi > 0$ exists such that $\omega \le -\Psi < 0$. Consequently, we have

$$
D^+\Xi(Z(t)) \le -\Psi \Xi(Z(t)) \tag{3.24}
$$

for all sufficiently large t. Hence, $T > 0$ exists such that, for all $t \ge T$, $\Xi(Z(t)) \le \Xi(Z(T))e^{-\Psi(t-T)}$. It follows that $\lim_{t\to\infty} \Xi(Z(t)) = 0$.

Following Proposition 4.1 of Sun and Loreau [38], which is based on the geometric approach of Li and Muldowney [54], the uniform exponential stability of the second additive compound system provides a sufficient contraction condition for the high-dimensional Bendixson criterion.

Under Assumption (H), this contraction condition holds along positive trajectories whenever the prescribed uniform bounds are valid. Consequently, non-trivial periodic orbits are excluded in the region where the geometric criterion applies, provided that its hypotheses are satisfied.

Together with the boundedness and uniform persistence results, the analysis above establishes a conditional geometric contraction criterion. Global convergence to the unique coexistence equilibrium E_3, however, requires verification of the complete hypotheses of the applicable Li–Muldowney global stability theorem. We summarize the result in the following proposition.

Proposition 7. *Suppose that System* (2.1) *is uniformly persistent and that Assumption* (H) *holds uniformly on a compact absorbing region contained in* $\mathrm{int}(\mathbb{R}^3_+)$. *Then the associated second additive compound variational system is uniformly exponentially stable along positive trajectories after they enter this region. Furthermore, if the geometric hypotheses of the Li–Muldowney high-dimensional Bendixson criterion are satisfied, the system admits no non-trivial periodic orbits contained in this region.*

Remark 5. *The conclusion of Proposition 7 is conditional on Assumption* (H) *and the hypotheses of the Li–Muldowney geometric framework. In particular, the negativity condition for the associated Lozinskiĭ measure provides a sufficient criterion for excluding non-trivial periodic solutions in the interior of the biologically feasible region. This conclusion should be distinguished from global asymptotic stability of the coexistence equilibrium E_3. A global convergence result requires the additional hypotheses of the corresponding global stability theorem to be established. Therefore, Proposition 7 is not interpreted as an unconditional global stability result over the entire biologically feasible region.*

Example 1. *On the basis of the local stability analysis in Subsection 3.2 and Proposition 7, we next carry out numerical simulations of the dynamics of S, I, and V to provide numerical evidence consistent with convergence toward the coexistence equilibrium E_3. We select the following parameters to illustrate the analytical findings mentioned above.*

$r = 0.5$, $K = 13$, $\beta_L = 0.016$, $\beta_T = 0.002$, $a_S = 0.025$, $a_I = 0.015$, $d_I = 0.2$, $d_V = 0.15$, $\gamma_S = 0.6$, $\gamma_I = 0.433$, $\eta_S = 0.002$, *and* $\eta_I = 0.001$.

The coexistence equilibrium is $E_3 = (S^*, I^*, V^*) = (11.2497, 0.6831, 1.1154)$. *The eigenvalues of the Jacobian matrix at* E_3 *are* $\lambda_1 = -0.4004$, $\lambda_2 = -0.0576$, *and* $\lambda_3 = -0.0114$. *Thus,* E_3 *is locally asymptotically stable.*

From the simulated trajectories, we record the numerical ranges $m_1 = 11.2270$, $m_2 = 0.6756$, $m_3 = 1.0108$, $\rho_1 = 11.3359$, $\rho_2 = 0.6848$, *and* $\rho_3 = 1.1434$. *These quantities represent numerically observed extrema along the selected trajectories and are not interpreted as uniform analytical bounds for all positive solutions.*

Using these numerically observed ranges, the coefficients appearing in Assumption (H) *are estimated as* $p_{11} = -0.4615$, $q_{12} = 0.0125$, $q_{13} = 0.3061$, $q_{21} = 0.0063$, $p_{22} = -0.4266$, $q_{23} = 0.6174$, $q_{31} = 0.0149$, $q_{32} = 0.0132$, *and* $p_{33} = -0.0327$. *Choose* $\delta_2 = 0.4849$ *and* $\delta_3 = 0.7237$. *Then*

$$G_1 = p_{11} + \frac{q_{12}}{\delta_2} + \frac{q_{13}}{\delta_3} = -0.0127 < 0,$$

$$G_2 = \delta_2 q_{21} + p_{22} + \frac{\delta_2}{\delta_3} q_{23} = -0.0099 < 0,$$

$$G_3 = \delta_3 q_{31} + \frac{\delta_3}{\delta_2} q_{32} + p_{33} = -0.0021 < 0,$$

Hence, for these numerically observed trajectory ranges, we have

$$\max\{G_1, G_2, G_3\} = -0.0021 < 0,$$

This numerical calculation is consistent with Assumption (H) *along the simulated trajectories. However, since the values m_i and ρ_i are obtained numerically rather than as uniform analytical bounds for all positive solutions, this computation should be interpreted as numerical support for the analytical criterion in Proposition 7, not as a rigorous verification of global asymptotic stability for the chosen parameter set.*

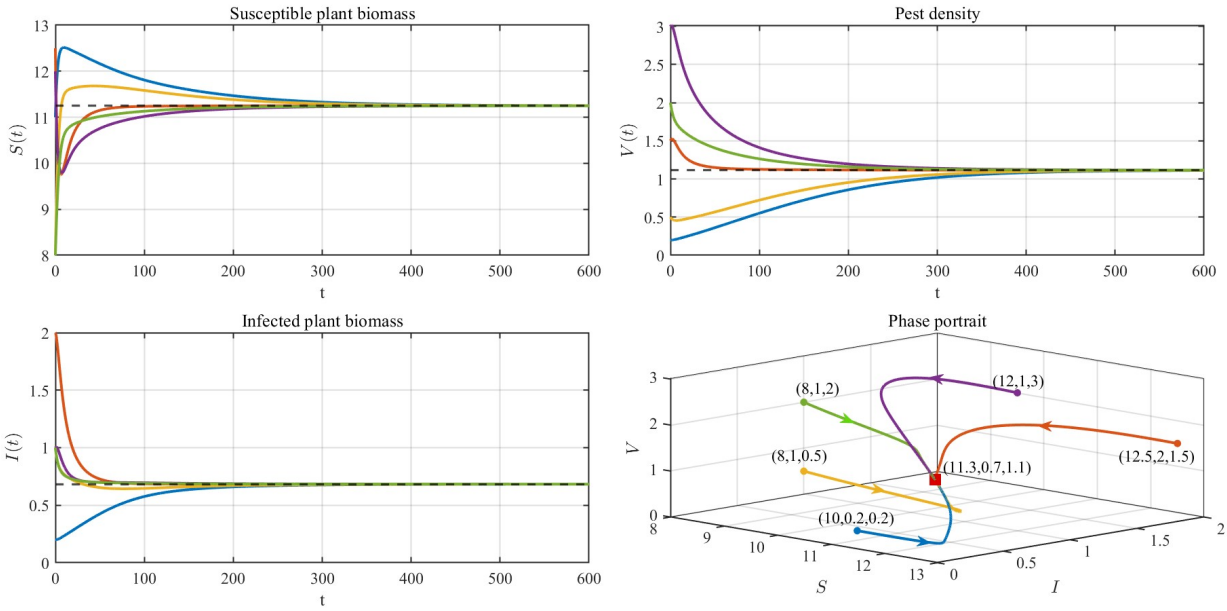


Figure 2. Time series of System (2.1) for several positive initial conditions, illustrating numerical convergence toward the coexistence equilibrium E_3.

Figure 2 shows that solutions starting from several positive initial conditions converge numerically to the coexistence equilibrium E_3. The dashed horizontal lines represent the equilibrium components S^*, I^*, and V^*. This numerical behavior is consistent with the local asymptotic stability of E_3 and illustrates convergence for the initial conditions considered. However, the simulated trajectories do not by themselves constitute a rigorous verification of the uniform bounds required in Assumption (H) *or establish global asymptotic stability.*

3.5. Bifurcation analysis

3.5.1. Transcritical bifurcation

Theorem 8. *Assume that $c_S K - d_V \neq 0$. System* (2.1) *undergoes a transcritical bifurcation involving the susceptible plant-only equilibrium $E_1 = (K, 0, 0)$ and the pest-free infected equilibrium $E_2 = (S_2, I_2, 0)$ when $\mathcal{R}_I = \frac{\beta_L K}{d_I} = 1$. The corresponding bifurcating equilibrium branch lies on the pest-free invariant subspace $V = 0$.*

Proof. Let $F(S, I, V; \mu) = (F_1, F_2, F_3)^T$ be the vector field of System (2.1), where $\mu = \beta_L K - d_I$ and $\beta_L = \frac{\mu + d_I}{K}$.

At $\mu = 0$, we have $\beta_L = d_I/K$. The Jacobian matrix at $E_1 = (K, 0, 0)$ is

$$J(E_1; 0) = \begin{pmatrix} -r & -r - d_I & -(\beta_T + a_S)K \\ 0 & 0 & \beta_T K \\ 0 & 0 & c_S K - d_V \end{pmatrix},$$

Since $c_S K - d_V \neq 0$, the Jacobian $J(E_1; 0)$ has a simple zero eigenvalue. The corresponding right and left eigenvectors are

$$v = \begin{pmatrix} -\dfrac{r + d_I}{r} \\ 1 \\ 0 \end{pmatrix}, \qquad w = \begin{pmatrix} 0 \\ 1 \\ -\dfrac{\beta_T K}{c_S K - d_V} \end{pmatrix},$$

We now verify the Sotomayor conditions. We obtain

$$\begin{aligned} w^T F_\mu(E_1; 0) &= 0, \\ w^T [DF_\mu(E_1; 0)v] &= 1 \neq 0, \\ w^T [D^2 F(E_1; 0)(v, v)] &= -\frac{2d_I(r + d_I)}{Kr} \neq 0, \end{aligned}$$

Therefore, by Sotomayor's theorem [45], System (2.1) undergoes a transcritical bifurcation at $E_1 = (K, 0, 0)$ when $\mathcal{R}_I = 1$. At this threshold, the equilibria E_1 and E_2 intersect, and the bifurcating equilibrium branch is contained in the pest-free invariant subspace $V = 0$. The two equilibria exchange stability with respect to the direct transmission direction.

In the full three-dimensional system, the remaining invasion eigenvalue is $c_S K - d_V$. Hence, the exchange in the direct transmission direction corresponds to an exchange of local asymptotic stability between E_1 and E_2 only when the pest density direction remains stable, namely $\mathcal{R}_V^{(1)} < 1$ at the bifurcation point. □

3.5.2. Bogdanov–Takens-type double-zero degeneracy

Remark 6. *The transcritical bifurcation at $E_1 = (K, 0, 0)$ is obtained when $\mathcal{R}_I = 1$, provided that the pest density invasion eigenvalue does not vanish. A codimension-two degeneracy occurs when $\mathcal{R}_I = 1$ and $\mathcal{R}_V^{(1)} = 1$ simultaneously.*

At this point, the Jacobian matrix at E_1 has one negative eigenvalue and a double-zero eigenvalue. Since the term $\beta_T KV$ appears in the linearized infected plant equation, the double-zero eigenvalue is nonsemisimple whenever $\beta_T > 0$. Hence, we have

$$(\beta_L, d_V) = \left(\frac{d_I}{K}, c_S K\right)$$

corresponds to a nonsemisimple double-zero eigenvalue and therefore identifies a candidate Bogdanov–Takens point. A complete classification as a Bogdanov–Takens bifurcation would require a center manifold reduction and verification of the corresponding normal-form nondegeneracy conditions, which are beyond the scope of the present study.

3.5.3. Hopf bifurcation

Theorem 9. *Assume that the positive coexistence equilibrium $E_3(d_V)$ exists and defines a smooth equilibrium branch in a neighborhood of $d_V = d_V^H$. System* (2.1) *exhibits a Hopf bifurcation around the positive coexistence equilibrium $E_3(d_V^H)$ when the pest mortality rate d_V crosses a critical value d_V^H, provided that*

$$\begin{aligned}
&\text{(i)} \quad K_1(d_V^H) > 0, \quad K_2(d_V^H) > 0,\\
&\text{(ii)} \quad \Delta_H(d_V^H) = K_1(d_V^H)K_2(d_V^H) - K_3(d_V^H) = 0,\\
&\text{(iii)} \quad \Delta_H'(d_V^H) \neq 0,
\end{aligned}$$

Proof. From the local stability analysis, the Jacobian matrix of System (2.1) at the coexistence equilibrium $E_3 = (S^*, I^*, V^*)$ is given in (3.15). Its characteristic equation is given in (3.16).

Since $E_3(d_V)$ defines a smooth equilibrium branch near $d_V = d_V^H$, the quantities $K_1(d_V)$, $K_2(d_V)$, and $K_3(d_V)$ depend smoothly on d_V along this branch.

Since d_V is chosen as the bifurcation parameter, the characteristic polynomial can be written as

$$p(\lambda, d_V) = \lambda^3 + K_1(d_V)\lambda^2 + K_2(d_V)\lambda + K_3(d_V),$$

At $d_V = d_V^H$, Condition (ii) gives

$$K_3(d_V^H) = K_1(d_V^H)K_2(d_V^H),$$

Therefore, at $d_V = d_V^H$, the characteristic equation becomes

$$\lambda^3 + K_1(d_V^H)\lambda^2 + K_2(d_V^H)\lambda + K_1(d_V^H)K_2(d_V^H) = 0,$$

This equation can be factorized as

$$\left(\lambda^2 + K_2(d_V^H)\right)\left(\lambda + K_1(d_V^H)\right) = 0,$$

Since $K_1(d_V^H) > 0$ and $K_2(d_V^H) > 0$, the eigenvalues are

$$\begin{aligned}
\lambda_1(d_V^H) &= -K_1(d_V^H) < 0,\\
\lambda_{2,3}(d_V^H) &= \pm i\sqrt{K_2(d_V^H)},
\end{aligned}$$

Thus, the Jacobian matrix at $E_3(d_V^H)$ has one negative real eigenvalue and a simple pair of purely imaginary eigenvalues.

It remains to verify the transversality condition. Let $\lambda(d_V) = \alpha(d_V) + i\omega(d_V)$ be one of the complex conjugate eigenvalues crossing the imaginary axis at d_V^H. At the critical value, we have $\alpha(d_V^H) = 0$ and $\omega(d_V^H) = \sqrt{K_2(d_V^H)}$.

Since $p(\lambda(d_V), d_V) = 0$, differentiating implicitly with respect to d_V gives

$$\frac{d\lambda}{dd_V} = -\frac{K_1'(d_V)\lambda^2 + K_2'(d_V)\lambda + K_3'(d_V)}{3\lambda^2 + 2K_1(d_V)\lambda + K_2(d_V)},$$

At $d_V = d_V^H$, substituting $\lambda = i\omega$, where $\omega = \sqrt{K_2(d_V^H)}$, and taking the real part yields

$$\left.\frac{d\alpha}{dd_V}\right|_{d_V=d_V^H} = -\frac{\Delta_H'(d_V^H)}{2\left(K_1^2(d_V^H) + K_2(d_V^H)\right)},$$

Since $K_1(d_V^H) > 0$ and $K_2(d_V^H) > 0$, the denominator is positive. Moreover, by Condition (iii), $\Delta_H'(d_V^H) \neq 0$. Therefore, we have

$$\left.\frac{d}{dd_V}\,\mathrm{Re}\,\lambda(d_V)\right|_{d_V=d_V^H} \neq 0,$$

Hence, the pair of complex conjugate eigenvalues crosses the imaginary axis with nonzero speed as d_V passes through d_V^H. This verifies the Hopf transversality condition.

Therefore, the Hopf bifurcation conditions are satisfied. By the Hopf bifurcation theorem [56], System (2.1) undergoes a Hopf bifurcation around the coexistence equilibrium $E_3(d_V^H)$. □

From a biological perspective, the Hopf bifurcation can be explained by the interactions among plant biomass, disease transmission, and the pest population's growth. An increase in pest density enhances herbivory and effective vector-mediated transmission, leading to a reduction in susceptible plant biomass and an increase in new infections. Changes in the susceptible and infected plant populations, in turn, affect pest growth through the term

$$(c_S S + c_I I - d_V)V,$$

When plant resources become limited and pest mortality exceeds recruitment, the pest population begins to decline. This reduction in pest density weakens herbivory and vector-mediated infection pressure, allowing susceptible plant biomass to recover under favorable conditions. The recovery of susceptible plants may subsequently support renewed pest growth, creating a feedback process that can give rise to oscillatory dynamics. At the Hopf bifurcation threshold, a pair of complex-conjugate eigenvalues crosses the imaginary axis, marking a change in the local stability of the coexistence equilibrium.

3.6. Global sensitivity analysis

The baseline parameter values used in the sensitivity analysis are given in Table 4. In total, 5000 parameter sets were generated using Latin hypercube sampling (LHS). The 12 model parameters r, K, β_L, β_T, a_S, a_I, d_I, d_V, γ_S, γ_I, η_S, and η_I were sampled from uniform distributions over the ranges specified in Table 2. No correlation structure was imposed among the sampled parameters. All 5000 sampled parameter sets were simulated successfully over $0 \le t \le 1200$ using the initial condition $(S(0), I(0), V(0)) = (40, 10, 5)$.

Partial rank correlation coefficients (PRCCs) are widely used for global sensitivity analysis of biological dynamic models with multiple uncertain parameters because they quantify the strength and direction of monotone associations between input parameters and model outputs while adjusting for the effects of the other parameters [57].

Because the model can exhibit oscillatory dynamics, the primary outputs were taken as the time-averaged state variables

$$\langle S\rangle = \frac{1}{600}\int_{600}^{1200} S(t)\,dt, \qquad \langle I\rangle = \frac{1}{600}\int_{600}^{1200} I(t)\,dt, \qquad \langle V\rangle = \frac{1}{600}\int_{600}^{1200} V(t)\,dt,$$

Table 2. Parameter ranges and distributions used in the LHS–PRCC analysis.

Parameter	Sampling range	Distribution
r	[0.005, 0.995]	Uniform
K	[1, 199]	Uniform
β_L	[0.00008, 0.01592]	Uniform
β_T	[0.0002, 0.0398]	Uniform
a_S	[0.0003, 0.0597]	Uniform
a_I	[0.00025, 0.04975]	Uniform
d_I	[0.001, 0.299]	Uniform
d_V	[0.003, 1.1]	Uniform
γ_S	[0.002, 0.398]	Uniform
γ_I	[0.009, 1.791]	Uniform
η_S	[0.00002, 0.00398]	Uniform
η_I	[0.00001, 0.00199]	Uniform

The terminal values $S(1200)$, $I(1200)$, and $V(1200)$ were retained only as secondary outputs for comparison.

The statistical significance of each PRCC was assessed using a two-sided test at the significance level $\alpha = 0.05$, and the 95% confidence intervals were estimated using 1000 bootstrap replicates. Following previous PRCC-based sensitivity studies [58–60], we use $|\text{PRCC}| > 0.4$ to indicate a relatively strong association. This threshold is used only to describe the magnitude of the association and is not interpreted as a criterion for statistical significance. Statistical significance is assessed separately at the 5% level.

The mean susceptible plant biomass $\langle S \rangle$ is particularly sensitive to the parameters β_L and d_I, with PRCC values -0.60451 and $+0.56311$, respectively (see Figure 3). Their 95% confidence intervals are $[-0.62527, -0.58284]$ and $[0.54108, 0.58512]$, respectively, and both associations are statistically significant at the 5% level. From the point of view of crop management, increasing β_L is associated with a reduction in the mean susceptible plant biomass because of increased direct disease transmission, whereas increasing d_I is associated with a higher mean susceptible plant biomass through faster removal of infected plant biomass.

Among the sampled parameters, the carrying capacity K shows the strongest positive association with the mean infected plant biomass $\langle I \rangle$, with PRCC $= +0.52547$ and a 95% confidence interval $[0.50447, 0.54719]$. This indicates that, over the sampled parameter region, larger plant carrying capacity is associated with greater time-averaged infected biomass. Several other parameters show weaker associations with $\langle I \rangle$, indicating that the infected plant dynamics are jointly influenced by ecological and epidemiological processes rather than by a single parameter.

The strongest association with the mean pest density $\langle V \rangle$ is observed for the pest mortality rate d_V, with PRCC $= -0.74424$ and a 95% confidence interval $[-0.75697, -0.72971]$. In addition, r, K, a_I, and γ_I show relatively strong positive associations with $\langle V \rangle$, with PRCC values $+0.45481$, $+0.48763$, $+0.46236$, and $+0.47007$, respectively. Thus, pest mortality exhibits the strongest negative rank-based association with time-averaged pest density over the prescribed sampling region.

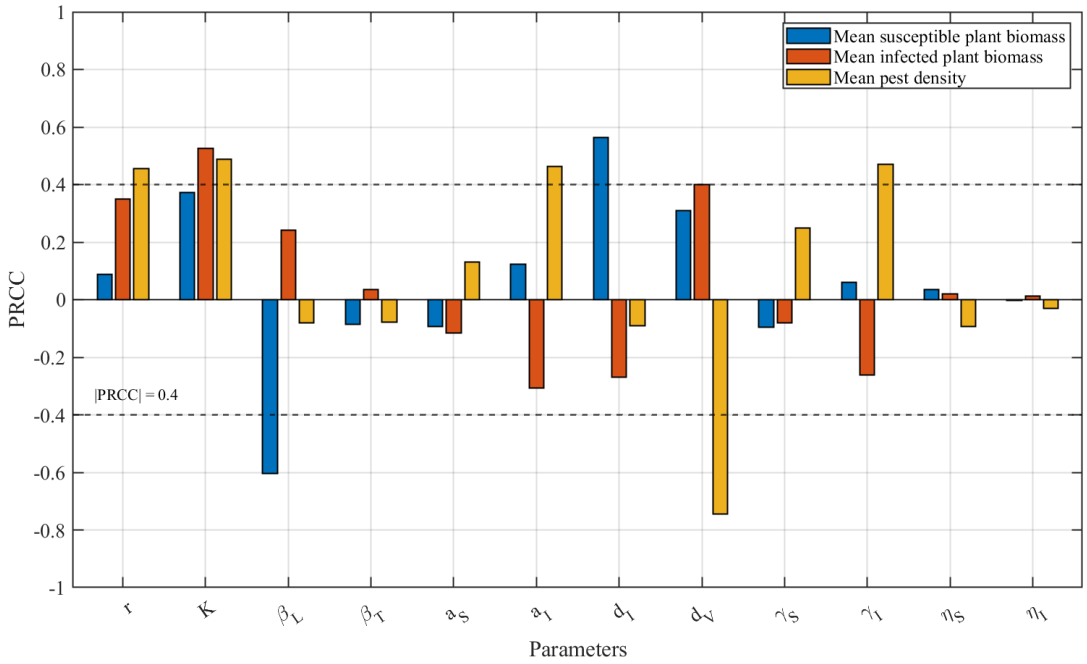


Figure 3. PRCC values of the model parameters for the time-averaged susceptible plant biomass, infected plant biomass, and pest density over the interval $600 \leq t \leq 1200$. The dashed lines at $|\text{PRCC}| = 0.4$ indicate relatively strong associations and do not represent a statistical significance threshold.

Table 3. Spearman rank-correlation diagnostics for parameter–output pairs exhibiting sign reversals between the lower and upper halves of the sampled parameter ranges.

Parameter	Output	ρ_s (lower)	ρ_s (upper)
d_V	$\langle S \rangle$	0.376364	−0.000372
η_S	$\langle S \rangle$	−0.003816	0.017043
β_L	$\langle I \rangle$	0.281361	−0.016240
η_S	$\langle I \rangle$	0.060978	−0.002609
η_I	$\langle I \rangle$	0.009253	−0.010944
β_L	$\langle V \rangle$	0.014079	−0.078679

To assess potential departures from monotonicity, Spearman rank correlations were computed separately for the lower and upper halves of each parameter's sampled values, using the sample median as the dividing point. Six of the 36 parameter–output pairs exhibited sign reversals (Table 3). However, several coefficients were close to zero, and the diagnostic represents marginal rather than partial correlations. Thus, these reversals suggest possible non-monotonicity but do not establish it.

Overall, the analysis identifies β_L and d_I as the principal parameters associated with $\langle S \rangle$, K as an important parameter for $\langle I \rangle$, and d_V as the dominant parameter associated with $\langle V \rangle$. These findings highlight the importance of disease transmission, infected plant removal, and pest mortality in the long-

term dynamics, subject to the prescribed parameter ranges and the limitations of rank-based sensitivity analysis.

4. Numerical simulations and biological interpretation

Numerical simulations are performed to connect the analytical findings with their biological interpretation and possible management implications. The simulations are organized to illustrate the threshold-driven transition associated with direct transmission on the pest-free invariant subspace, the codimension-two interaction between the direct transmission and pest density invasion thresholds, the emergence of oscillatory coexistence through a Hopf bifurcation, the role of vector-mediated transmission, and the stabilizing effect of allomone-mediated pest suppression.

Unless otherwise stated, the numerical simulations use the baseline parameter values listed in Table 4. These values are selected for illustrative dynamic exploration rather than calibration to a specific crop–pest system. To investigate the sensitivity of the model and its bifurcation behavior, selected parameters are varied around their baseline values, particularly the direct transmission rate β_L, the pest mortality rate d_V, and the effective vector-mediated transmission rate β_T. The effects of the allomone parameters η_S and η_I, which reduce the net pest growth coefficients c_S and c_I, are also examined.

Table 4. Baseline parameter values used in the numerical simulations.

Parameter	r	K	β_L	β_T	a_S	a_I	d_I	d_V	γ_S	γ_I	η_S	η_I
Value	0.5	100	0.008	0.02	0.03	0.025	0.1	0.3	0.2	0.9	0.002	0.001

4.1. Feasibility and local stability of coexistence equilibria

To examine the biological feasibility and local stability of the coexistence equilibrium, we consider two parameter sets. Set A uses the baseline parameters in Table 4, whereas Set B differs only in the effective vector-mediated transmission coefficient $\beta_T = 0.0001$ and the pest mortality rate $d_V = 0.25$. All other parameters remain unchanged. The results are illustrated in Figure 4.

For Set A, we obtain $c_S = 0.004$, $c_I = 0.0215$, and $d_V/c_S = 75$. Equation (3.1) admits two positive roots, $S_1^* \approx 97.0834$ and $S_2^* \approx 13.4980$. The first root gives $I_1^* \approx -4.1085$ and $V_1^* \approx 1.3599$, and is therefore biologically inadmissible. The second root satisfies the positivity conditions and yields the feasible coexistence equilibrium $E_3^{(A)} \approx (13.4980, 11.4422, 5.6752)$. Evaluating the characteristic coefficients at this equilibrium gives $K_1 \approx 0.201387$, $K_2 \approx 0.062301$, and $K_3 \approx 0.019005$, with $K_1K_2 - K_3 \approx -0.006458 < 0$. The corresponding eigenvalues are $\lambda_{1,2} \approx 0.0256 \pm 0.2731\mathrm{i}$ and $\lambda_3 \approx -0.2526$. Since the complex-conjugate pair has positive real parts, $E_3^{(A)}$ is locally unstable.

For Set B, the positivity threshold becomes $d_V/c_S = 62.5$. Equation (3.1) again admits two positive roots, $S_1^* \approx 63.3296$ and $S_2^* \approx 37.7451$. The first root gives $I_1^* \approx -0.1543$ and $V_1^* \approx 6.1581$, and is therefore biologically inadmissible. The second root yields the feasible coexistence equilibrium $E_3^{(B)} \approx (37.7451, 4.6056, 8.3522)$. The characteristic coefficients are $K_1 \approx 0.195571$, $K_2 \approx 0.077736$, and $K_3 \approx 0.009896$, satisfying $K_1K_2 - K_3 \approx 0.005307 > 0$. The corresponding eigenvalues are $\lambda_{1,2} \approx -0.0272 \pm 0.2633\mathrm{i}$ and $\lambda_3 \approx -0.1412$. Hence, the Routh–Hurwitz conditions are satisfied, and $E_3^{(B)}$ is locally asymptotically stable.

The comparison shows that, for each parameter set, Equation (3.1) admits two positive algebraic roots, but only one satisfies the biological feasibility conditions $S^* > 0$, $I^* > 0$, and $V^* > 0$. The feasible coexistence equilibrium is locally unstable for Set A and locally asymptotically stable for Set B. Since these results correspond to different parameter settings, they do not establish bistability. These findings are illustrated by the feasibility profiles in Figure 4(a) and the eigenvalue distributions in Figure 4(b).

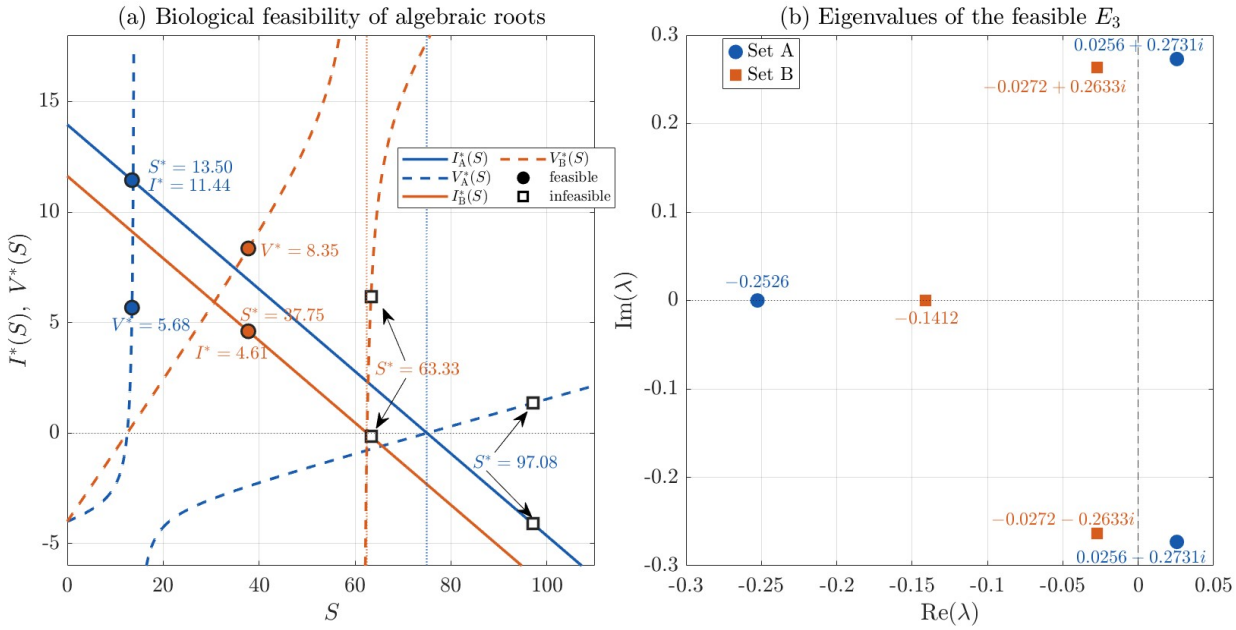


Figure 4. Biological feasibility and local stability of coexistence equilibria under two parameter sets. (a) Feasibility profiles $I^*(S)$ and $V^*(S)$, together with the infected plant positivity thresholds $S = d_V/c_S$. Filled circles indicate biologically feasible roots, whereas open squares indicate infeasible roots. (b) Eigenvalues of the Jacobian at the feasible coexistence equilibria, showing local instability for Set A and local asymptotic stability for Set B.

These numerical results are consistent with the analytical root classification in Subsection 3.1.1 and the local stability criterion established in Subsection 3.2.

4.2. Threshold-driven transition governed by $\mathcal{R}_I$

To examine the analytical transcritical bifurcation result, the direct transmission rate β_L is varied while the remaining parameters are fixed at the values given in Table 4. According to Theorem 8, the susceptible plant-only equilibrium $E_1 = (K, 0, 0)$ and the pest-free infected equilibrium $E_2 = (S_2, I_2, 0)$ intersect when $\mathcal{R}_I = 1$. For the parameter set used in the simulation, this threshold is $\beta_L^* = \frac{d_I}{K} = 0.0010$.

The transcritical bifurcation diagram with respect to β_L is shown in Figure 5(a). The red solid branch represents the stable susceptible plant-only equilibrium E_1, while the red dashed branch represents the unstable part of E_1 after the threshold is crossed. The blue solid branch represents the stable pest-free infected equilibrium E_2. The vertical dash-dotted line marks the critical value $\beta_L^* = d_I/K = 0.0010$, or equivalently $\mathcal{R}_I = 1$. Thus, the numerical bifurcation diagram confirms the exchange of stability between E_1 and E_2 on the pest-free invariant subspace $V = 0$, in agreement with the analytical result.

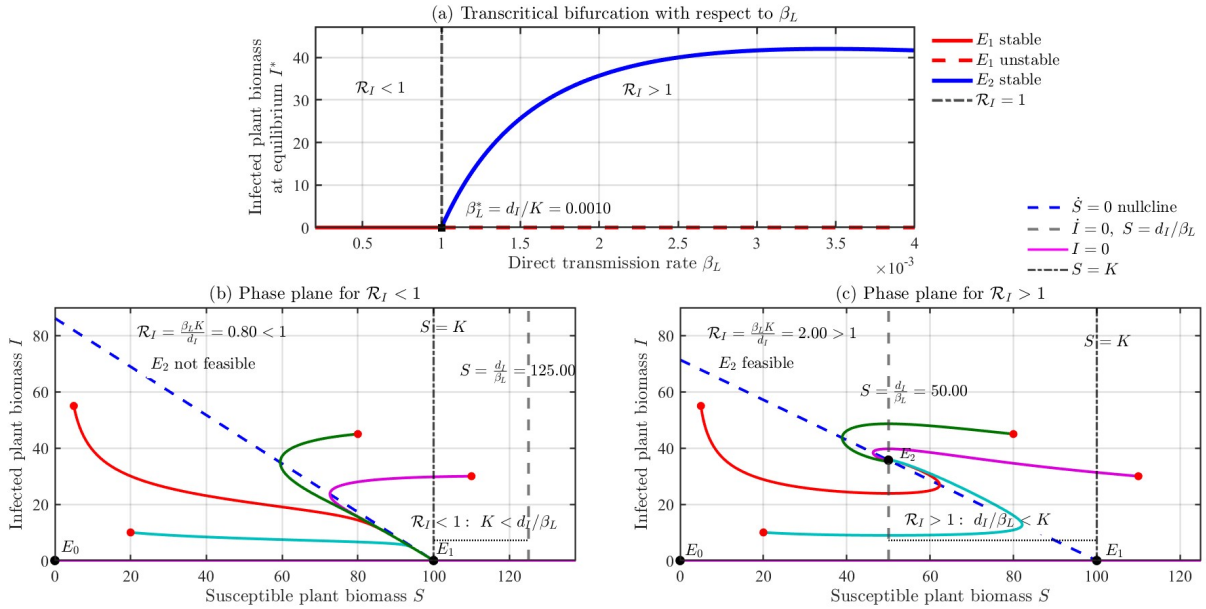


Figure 5. Bifurcation governed by the direct transmission threshold $\mathcal{R}_I$. Panel (a) shows the bifurcation diagram with respect to β_L, where $\beta_L^* = d_I/K$ corresponds to $\mathcal{R}_I = 1$. Panels (b) and (c) show the pest-free phase plane dynamics for $\mathcal{R}_I < 1$ and $\mathcal{R}_I > 1$, respectively.

More specifically, when $\mathcal{R}_I < 1$, the infected equilibrium E_2 is not biologically feasible, and the system approaches E_1 within the pest-free subsystem. When $\mathcal{R}_I > 1$, the susceptible plant-only equilibrium E_1 loses stability, while E_2 becomes feasible and locally stable in the pest-free subsystem. For example, when $\beta_L = 0.0002$, one obtains $\mathcal{R}_I = 0.2$, and E_2 is not biologically feasible. At the threshold value $\beta_L = 0.0010$, we obtain $\mathcal{R}_I = 1$, $S_2 = 100.0000$, and $I_2 = 0$. When $\beta_L = 0.0022$, one obtains $\mathcal{R}_I = 2.2$ and $E_2 = (45.4550, 37.8790, 0)$. Furthermore, when $\beta_L = 0.004$, one obtains $\mathcal{R}_I = 4$ and $E_2 = (25.0000, 41.6670, 0)$. For the baseline value $\beta_L = 0.008$, the pest-free infected equilibrium becomes $E_2 = (12.5000, 33.6540, 0)$, whereas for $\beta_L = 0.012$, it is $E_2 = (8.3333, 26.9610, 0)$. These values show that, once the threshold is crossed, infected plant biomass can persist in the pest-free subsystem. Over the numerical branch considered, the infected component reaches its maximum approximately at $\beta_L = 0.0034477064$, $\mathcal{R}_I = 3.4477064220$, and $I_2 = 42.0204057004$. Beyond this point, I_2 decreases slightly because the susceptible component $S_2 = d_I/\beta_L$ becomes smaller as β_L increases.

Figures 5(b)–(c) illustrate the dynamics on the pest-free plane $V = 0$. The blue dashed curve represents the $\dot{S} = 0$ nullcline, the gray dashed vertical line denotes the $\dot{I} = 0$ nullcline $S = d_I/\beta_L$, and the black dash-dotted line indicates $S = K$. The relative positions of these nullclines determine the biological feasibility of the pest-free infected equilibrium E_2.

For $\mathcal{R}_I < 1$, with $\beta_L = 0.0008$, we obtain $\mathcal{R}_I = 0.80$ and $d_I/\beta_L = 125 > K = 100$ (Figure 5(b)). Consequently, E_2 is biologically infeasible, while $E_1 = (100, 0, 0)$ is locally asymptotically stable within the pest-free subsystem, with a maximum real eigenvalue of -0.0200. Numerical trajectories from different initial conditions approach E_1, consistent with the extinction of infected plant biomass on the pest-free plane.

For $\mathcal{R}_I > 1$, with $\beta_L = 0.0020$, we obtain $\mathcal{R}_I = 2.00$ and $d_I/\beta_L = 50 < K = 100$ (Figure 5(c)). In this case, the feasible equilibrium $E_2 = (50.0000, 35.7140, 0)$ is locally asymptotically stable within the pest-free subsystem, with the eigenvalues having the real parts -0.1250, whereas E_1 is unstable, with a maximum real eigenvalue of 0.1000. Numerical trajectories converge to E_2, confirming the persistence of infected plant biomass on the pest-free plane.

The preceding simulation shows that the direct transmission rate β_L controls the ability of infected plant biomass to invade the susceptible plant-only equilibrium through the threshold $\mathcal{R}_I = 1$. However, the local stability of $E_1 = (K, 0, 0)$ is also affected by pest density invasion through the threshold $\mathcal{R}_V^{(1)} = 1$. Therefore, it is natural to examine the joint variation of β_L and d_V in order to visualize how the two invasion thresholds interact in the (β_L, d_V)-plane.

4.3. Codimension-two threshold interaction in the (β_L, d_V)-plane

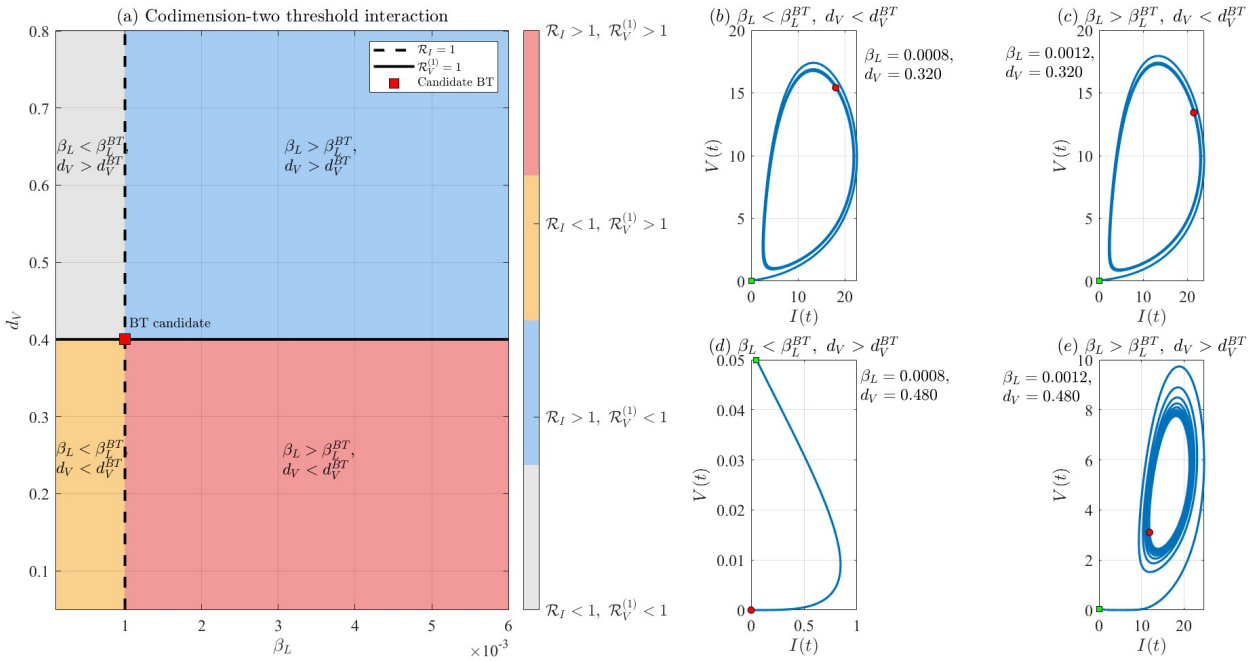


Figure 6. Codimension-two threshold interaction and local dynamics near the candidate Bogdanov–Takens point. (a) The (β_L, d_V)-plane divided by the threshold curves $\mathcal{R}_I = 1$ and $\mathcal{R}_V^{(1)} = 1$, whose intersection gives the codimension-two threshold point. (b)–(e) Local phase portraits near $E_1 = (K, 0, 0)$ for parameter values below and above the two critical thresholds.

The threshold structure associated with the codimension-two interaction near the susceptible plant-only equilibrium $E_1 = (K, 0, 0)$ is summarized in Figure 6.

Figure 6(a) shows that the threshold curves $\mathcal{R}_I = 1$ and $\mathcal{R}_V^{(1)} = 1$ divide the (β_L, d_V) plane into four regions, corresponding to the four possible combinations of infection invasion and pest density invasion. Their intersection occurs at $(\beta_L, d_V) = \left(\frac{d_I}{K}, c_S K\right) = (0.0010, 0.4000)$, which gives the candidate Bogdanov–Takens point.

At this candidate point, the Jacobian matrix at E_1 has the eigenvalues $\lambda_1 = -0.5000$, $\lambda_2 = 0.0000$, and $\lambda_3 = 0.0000$. The rank of J at the candidate point is 2, the rank of J^2 at the candidate point is 1, and

the nullity of J at the candidate point is 1. Because $\beta_T K = 2.0000$ is nonzero, the zero eigenvalue is not semisimple. Thus, E_1 has a double-zero eigenvalue with Jordan-type degeneracy. This is a numerical indication of a Bogdanov–Takens candidate point.

The four surrounding regions have clear biological interpretations. In the region $\mathcal{R}_I < 1$ and $\mathcal{R}_V^{(1)} < 1$, neither the direct transmission infection mode nor the pest density mode can invade E_1. In the region $\mathcal{R}_I > 1$ and $\mathcal{R}_V^{(1)} < 1$, the direct transmission infection mode can invade, whereas pest density cannot. In the region $\mathcal{R}_I < 1$ and $\mathcal{R}_V^{(1)} > 1$, direct transmission alone is below its invasion threshold, but pest density can invade E_1. Because $\beta_T > 0$, such pest invasion generates infected plant biomass through the vector-mediated term $\beta_T S V$, even though $\mathcal{R}_I < 1$. Finally, in the region $\mathcal{R}_I > 1$ and $\mathcal{R}_V^{(1)} > 1$, both the direct transmission infection mode and the pest density mode are locally invasive.

Figure 6(b)–(e) illustrates the corresponding local phase portraits near E_1. These panels confirm that crossing $\beta_L = \beta_L^{BT}$ changes the sign of the direct transmission invasion eigenvalue, whereas crossing $d_V = d_V^{BT}$ changes the sign of the pest density invasion eigenvalue. Hence, the intersection of these two threshold curves organizes the local invasion dynamics around E_1.

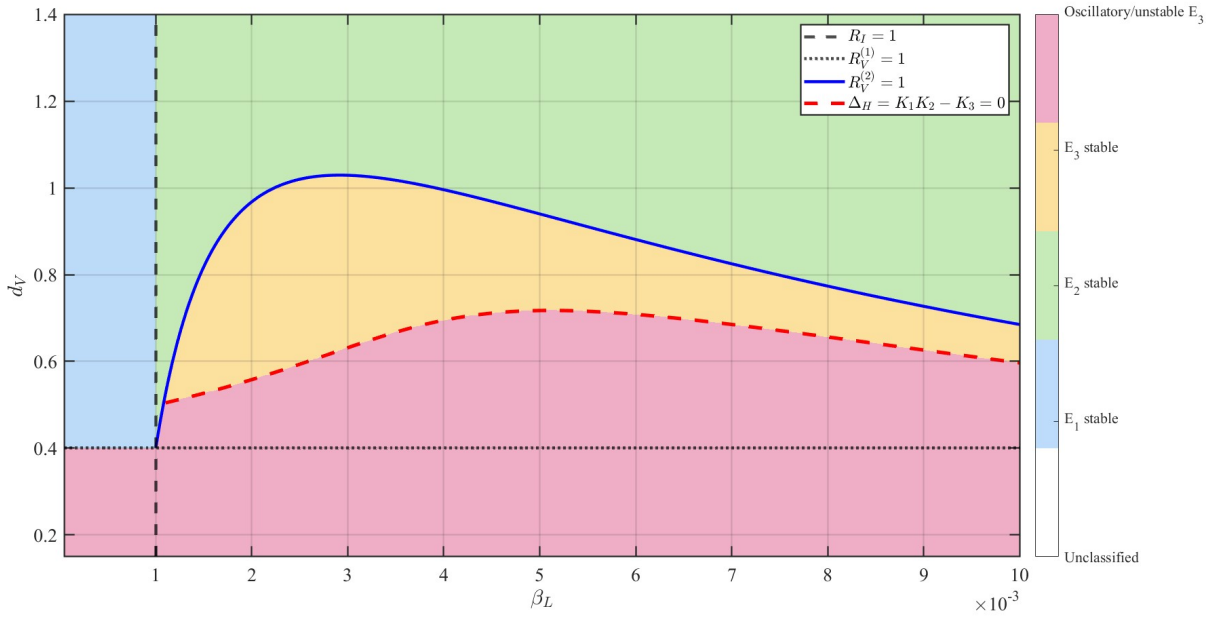


Figure 7. Two-parameter region diagram in the (β_L, d_V)-plane showing different dynamic regimes of System (2.1).

While Figure 6 illustrates the local threshold geometry and invasion directions near the susceptible plant-only equilibrium $E_1 = (K, 0, 0)$, Figure 7 provides a broader numerical classification of the long-term dynamics of System (2.1) in the (β_L, d_V)-plane.

The direct transmission rate β_L determines the direct transmission invasion threshold. However, $\mathcal{R}_I < 1$ does not necessarily imply disease extinction in the full system, since persistent pest populations may sustain infection through the vector-mediated term $\beta_T S V$. When direct transmission exceeds its invasion threshold, infection can persist through the direct pathway, while the resulting dynamic regime also depends on pest persistence.

The pest mortality rate d_V influences both pest persistence and coexistence stability. In the parameter regions examined, lower d_V favors persistent pest populations and oscillatory dynamics, whereas higher d_V suppresses pest density and promotes stable coexistence or pest exclusion. Together, these results indicate that reducing direct transmission and increasing pest mortality may help limit infection and pest outbreaks, although disease persistence also depends on the vector-mediated pathway.

4.4. Hopf bifurcation governed by pest mortality d_V

To verify the Hopf bifurcation result, the pest mortality rate d_V is varied around the critical value d_V^H, while the remaining parameters are fixed as shown in Table 4. The analytical condition $K_1K_2 - K_3 = 0$ indicates that Hopf bifurcation occurs when a pair of complex conjugate eigenvalues crosses the imaginary axis. For the present parameter set, the critical value is $d_V^H \approx 0.6562$, and three representative values are considered: $d_V = 0.6262 < d_V^H$, $d_V = 0.6562 \approx d_V^H$, and $d_V = 0.6862 > d_V^H$.

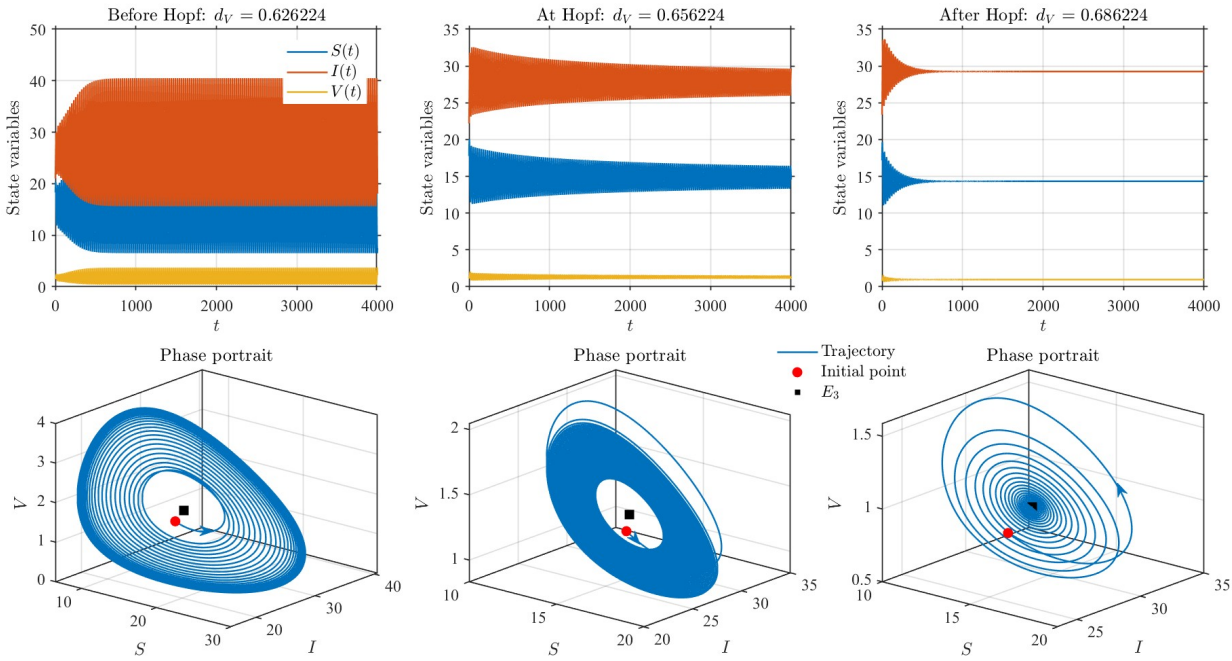


Figure 8. Time series and phase portraits before, near, and after the Hopf bifurcation point d_V^H.

Figure 8 shows the dynamic transition as d_V crosses d_V^H. For $d_V = 0.6262 < d_V^H$, the solution exhibits sustained oscillations, and the phase portraits form closed orbits around E_3, indicating the coexistence of oscillations. Near $d_V = 0.6562$, small-amplitude oscillations appear around the coexistence equilibrium, consistent with the Hopf condition. For $d_V = 0.6862 > d_V^H$, the oscillations dampen, and the trajectories converge to E_3, indicating that the coexistence equilibrium becomes locally asymptotically stable after the Hopf threshold is exceeded.

Biologically, low pest mortality allows pest density, herbivory, and disease transmission to generate recurrent outbreaks, while increasing d_V beyond d_V^H suppresses pest persistence and stabilizes the plant–pest–disease system.

To complement the selected trajectories in Figure 8, Figure 9 presents a one-parameter bifurca-

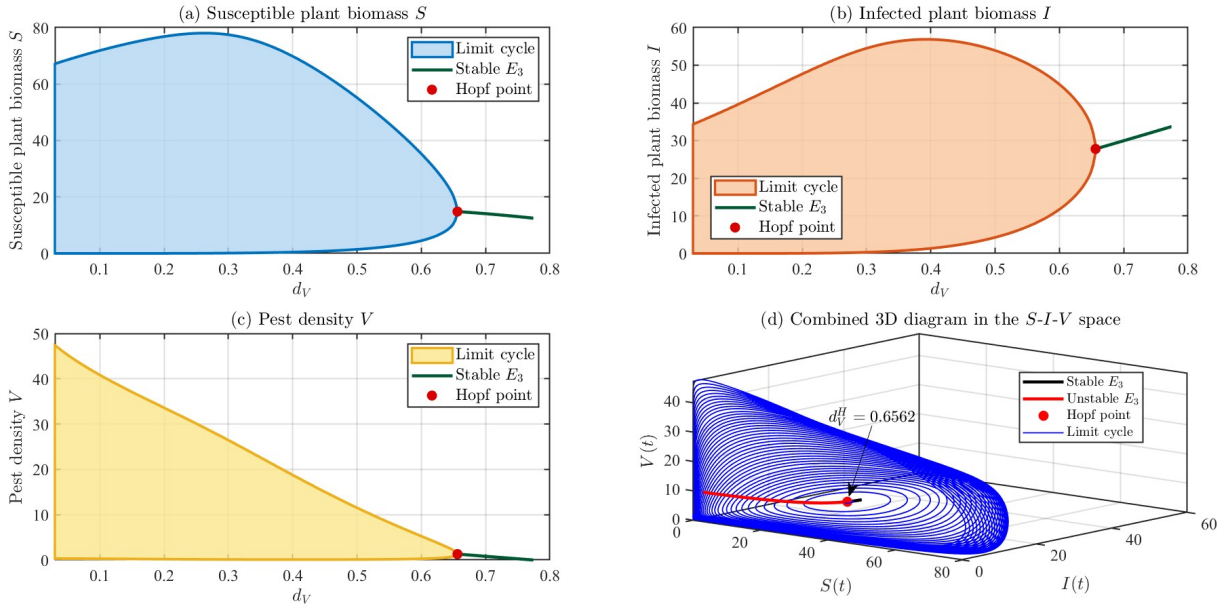


Figure 9. Hopf bifurcation diagram with respect to the pest mortality rate d_V. The critical value d_V^H separates oscillatory coexistence from stable coexistence.

tion diagram with respect to d_V. The Hopf threshold is obtained at $d_V^H = 0.6562$, with $E_3(d_V^H) = (14.8251, 27.7639, 1.2989)$. At this point, $K_1 = 0.0880$, $K_2 = 0.0638$, $K_3 = 0.0056$, and $K_1K_2 - K_3 = -7.5460\times10^{-17} \approx 0$. The corresponding eigenvalues are $\lambda_1 = -0.0880$ and $\lambda_{2,3} = \pm 0.2526i$, confirming the Hopf bifurcation criterion.

The diagram shows that sustained oscillations occur for $d_V < d_V^H$, whereas for $d_V > d_V^H$, the oscillations disappear and the solution converges to the stable coexistence equilibrium. Hence, the Hopf threshold marks the transition from oscillatory coexistence to stable coexistence, emphasizing the stabilizing role of pest mortality.

4.5. Effect of vector-mediated transmission

To examine the effect of vector-mediated transmission, β_T is varied while the other parameters are fixed as shown in Table 4. Figure 10 shows that increasing β_T changes the long-term interaction between pest density $V(t)$ and infected plant biomass $I(t)$.

For weak vector-mediated transmission, $\beta_T = 0.0001$, the trajectories in Figure 10(a) converge to the stable coexistence equilibrium $E_3 \approx (35.5842, 7.3332, 7.5332)$, corresponding to $(V_3, I_3) \approx (7.5332, 7.3332)$ in the (V, I)-plane.

This indicates that, for sufficiently small β_T, the pest–infection dynamics converge to a stable coexistence equilibrium. In contrast, when $\beta_T = 0.0200$, the coexistence equilibrium E_3 becomes unstable, with $\max\{\mathrm{Re}(\lambda_i)\} \approx 0.0256$. As shown in Figure 10(b), the trajectories approach a stable periodic orbit surrounding E_3, resulting in sustained oscillations in infected plant biomass and pest density.

Figure 10(c), (d) confirm that this transition is caused by a Hopf bifurcation at $\beta_T^H \approx 0.005897$, where $E_3(\beta_T^H) \approx (22.6889, 9.7323, 7.2439)$. At this point, $\Delta = K_1K_2 - K_3 \approx -2.1014 \times 10^{-13} \approx 0$, and

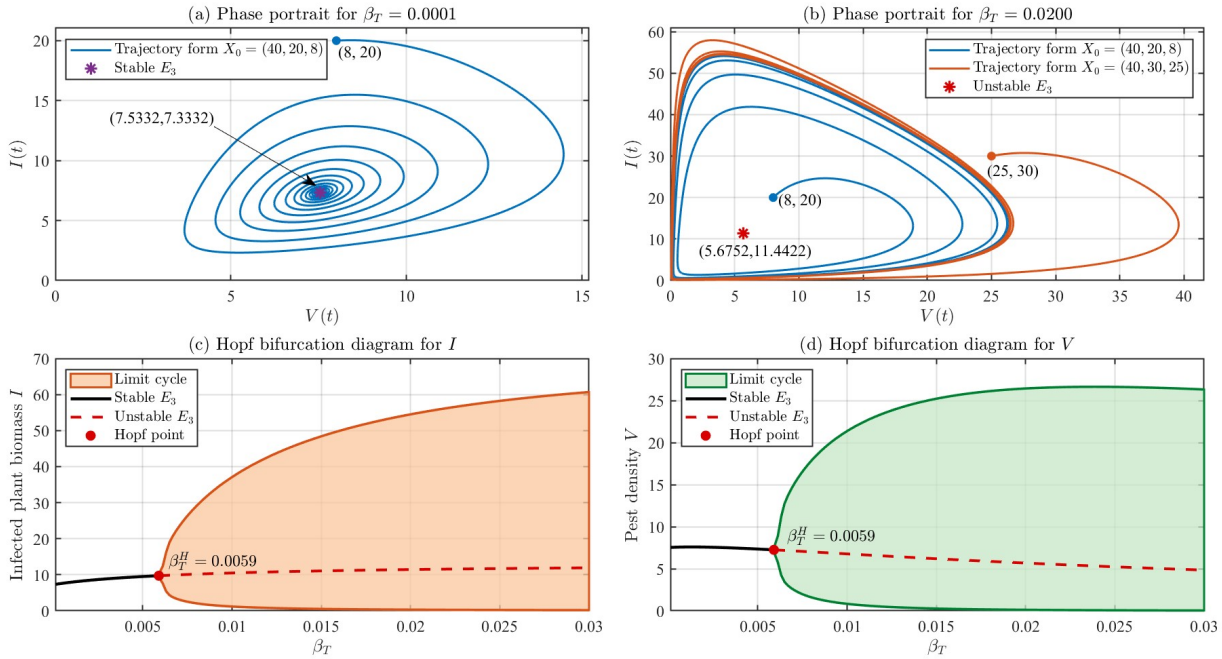


Figure 10. Effects of vector-mediated transmission on phase dynamics and Hopf bifurcation. (a)–(b) show the (V, I) phase portraits for $\beta_T = 0.0001$ and $\beta_T = 0.0200$, respectively. (c)–(d) present the Hopf bifurcation diagrams for infected plant biomass I and pest density V with respect to β_T, with a critical Hopf point at $\beta_T^H \approx 0.005897$.

the eigenvalues are $\lambda_{1,2} \approx \pm 0.2958i$ and $\lambda_3 \approx -0.2130$.

To determine the criticality of the Hopf bifurcation with respect to β_T, the first Lyapunov coefficient was evaluated numerically at $\beta_T = \beta_T^H$ using the standard Hopf normal-form formula. The result $l_1 \approx -5.96 \times 10^{-5} < 0$ confirms that the Hopf bifurcation is supercritical, with a stable small-amplitude periodic orbit emerging as the coexistence equilibrium loses stability.

Biologically, increasing β_T strengthens the vector-mediated transmission feedback through the term $\beta_T VS$. As β_T crosses β_T^H, this feedback destabilizes the coexistence equilibrium and generates sustained oscillations in infected plant biomass and pest density.

4.6. Allomone-mediated pest suppression and stabilization effects

To assess the role of allomone-mediated pest suppression, the parameters η_S and η_I are varied while the remaining parameters are fixed as in Table 4. Since η_S and η_I reduce the net pest growth coefficients c_S and c_I, larger allomone effects weaken the contribution of plant biomass to the pest population's growth. The simulations are restricted to the modeling assumption $\eta_S > \eta_I$.

Figure 11(a) shows that stronger allomone-mediated suppression reduces pest density $V(t)$ and changes the long-term dynamics. Under weak allomone effects, $E_3 \approx (16.0410, 21.4250, 2.8255)$ is unstable with $\max\{\mathrm{Re}(\lambda_i)\} \approx 0.0128$, leading to persistent oscillations. For moderate allomone effects, the system approaches a stable coexistence equilibrium $E_3 \approx (13.4440, 31.5280, 0.4583)$, while strong allomone effects make the interior equilibrium infeasible and nearly eliminate pests, with $V(T) \approx 9.0634 \times 10^{-12}$.

Figure 11(b) shows that suppressing pests does not always reduce infected biomass $I(t)$, because pests both transmit infection through $\beta_T S V$ and reduce infected plants through herbivory $-a_I I V$. Thus, when pest density decreases, herbivory pressure on infected plants weakens and $I(t)$ may increase due to direct transmission $\beta_L S I$.

Figure 11(c) summarizes the stability regions in the (η_S, η_I)-plane. Weak allomone effects support oscillatory coexistence, moderate effects stabilize the coexistence equilibrium E_3, and strong effects drive the system toward pest exclusion and the pest-free infected equilibrium E_2.

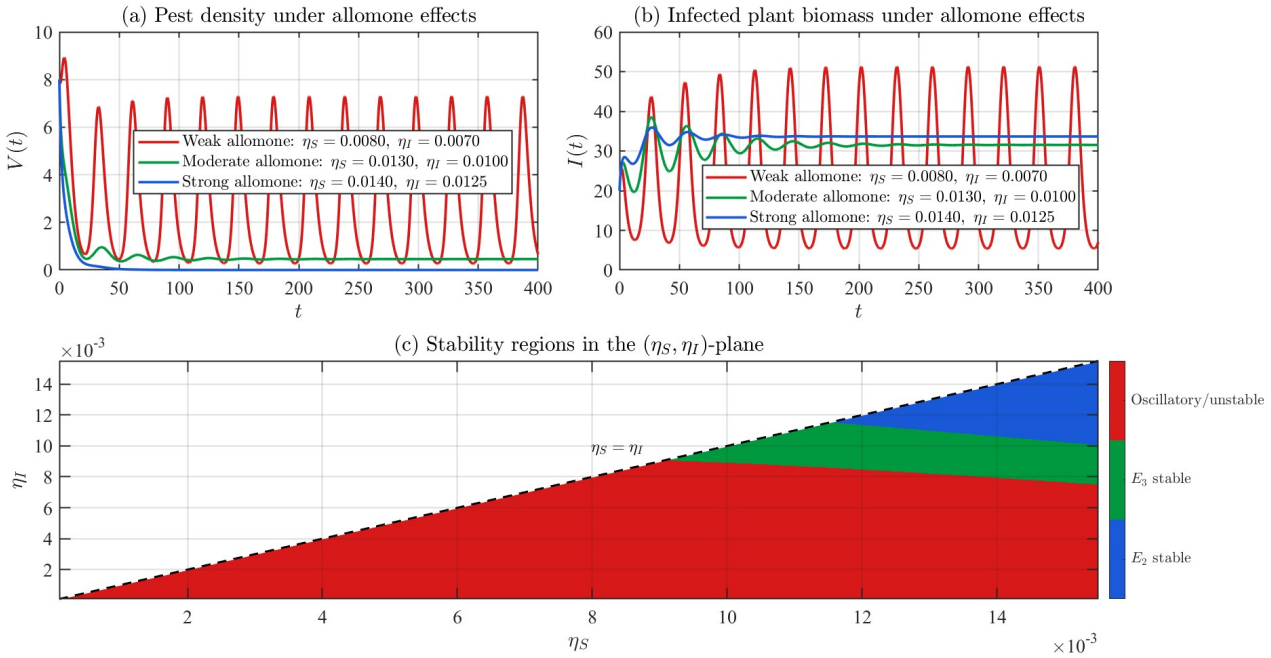


Figure 11. Effects of allomone-mediated pest suppression under $\eta_S > \eta_I$. (a)–(b) The responses of $V(t)$ and $I(t)$ under weak, moderate, and strong allomone effects; (c) the corresponding stability regions in the (η_S, η_I)-plane.

4.7. Combined parameter effects on dynamic regions

Additionally, Figure 12 shows two-parameter dynamic regions involving the allomone parameters η_S and η_I together with β_T, d_V, and β_L. Figure 12(a), (b) shows that increasing β_T can enlarge the region of oscillatory coexistence, whereas larger η_S and η_I reduce the net pest growth coefficients c_S and c_I and tend to stabilize the dynamics. Figure 12(c), (d) shows that allomone-mediated suppression and pest mortality d_V work together to reduce pests' persistence and dampen oscillations. Figure 12(e), (f) shows that, when the direct transmission coefficient β_L is large, infection can persist even under stronger pest suppression, whereas for smaller β_L, the allomone effect is more effective in stabilizing the system. These dynamic findings motivate the introduction of treatment and insecticide controls in the next section.

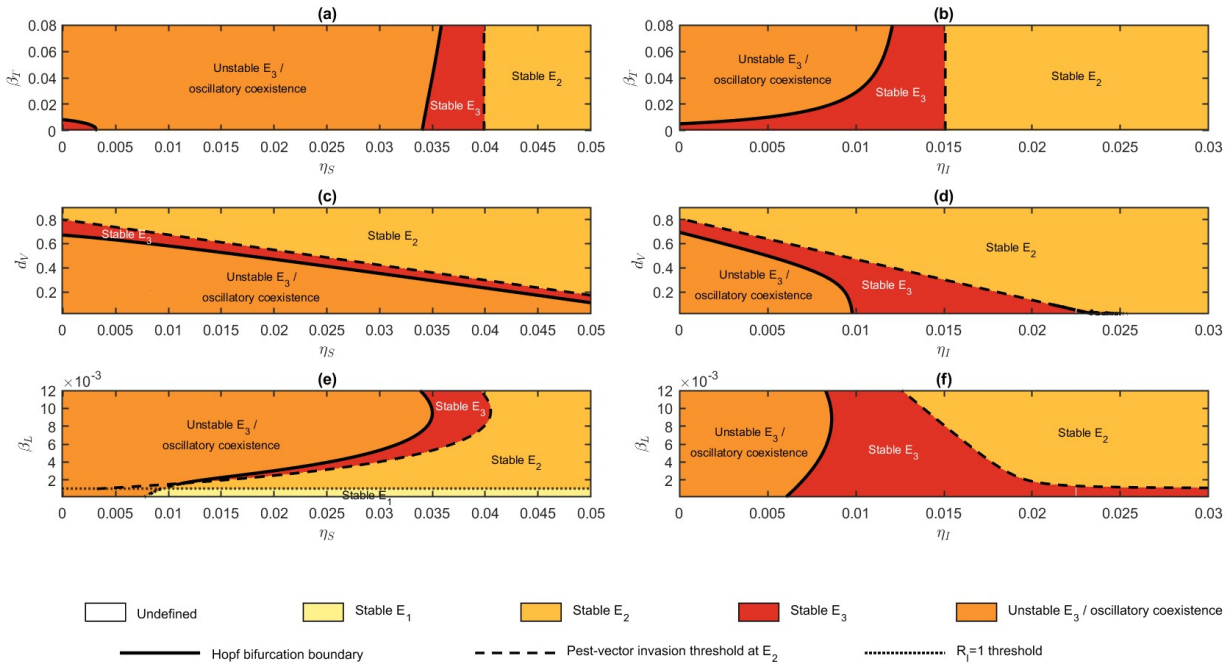


Figure 12. Two-parameter dynamic regions of Model (2.1). Panels (a)–(f) illustrate the combined effects of the allomone parameters η_S and η_I with β_T, d_V, and β_L. The colored regions indicate the numerically identified dynamic regimes, while the black curves indicate the corresponding threshold and numerically determined Hopf boundaries.

5. Optimal control problem

5.1. Solving the optimal control problem

In this section, the uncontrolled model is extended to an optimal control problem in order to reduce infected plant biomass and pest density during a fixed time interval $[0, T]$. Two time-dependent control variables are introduced. The first control, $u_1(t)$, represents an externally applied treatment that promotes the recovery of infected plant biomass, while the second control, $u_2(t)$, represents insecticide application for suppressing pest density. Accordingly, the term $-u_1(t)I(t)$ reduces the infected plant biomass, while the corresponding term $+u_1(t)I(t)$ transfers the successfully treated biomass back to the susceptible class. This formulation does not imply the spontaneous recovery of infected plants; rather, recovery occurs as a consequence of the applied treatment. The recovered plant biomass is assumed not to acquire permanent immunity and therefore returns to the susceptible class, where it may become infected again through direct or vector-mediated transmission. Thus, $u_1(t)$ represents a recovery-oriented treatment rather than roguing or removal of infected plants. The insecticide control $u_2(t)$ increases pest mortality through the term $-u_2(t)V(t)$.

The controlled system is given by

$$\begin{aligned}
\frac{dS}{dt} &= rS\left(1-\frac{S+I}{K}\right)-(\beta_L I+\beta_T V)S-a_S SV+u_1(t)I,\\
\frac{dI}{dt} &= (\beta_L I+\beta_T V)S-a_I IV-d_I I-u_1(t)I,\\
\frac{dV}{dt} &= c_S SV+c_I IV-d_V V-u_2(t)V,
\end{aligned} \tag{5.1}$$

The present control formulation focuses on two intervention pathways: Treatment of infected plant biomass and insecticide-induced suppression of the pest population. Although the insecticide control $u_2(t)$ indirectly reduces vector-mediated transmission by decreasing the pest density $V(t)$, it does not directly modify the transmission coefficient β_T.

A separate control acting directly on the vector-mediated transmission term $\beta_T VS$, for example, by reducing the vector's competence, vector–plant contact, or transmission efficiency, is not considered in the present study. Such an intervention would require an additional control variable and a corresponding extension of the objective functional. This possibility is left for future extensions of the model.

With the initial conditions $X(0) = X_0 = (S_0, I_0, V_0)$, the admissible control set is defined by

$$\mathcal{U} = \{(u_1, u_2) : 0 \le u_1(t) \le u_{1,\max},\ 0 \le u_2(t) \le u_{2,\max}, t \in [0, T]\}, \tag{5.2}$$

Here, $u_{1,\max}$ and $u_{2,\max}$ denote the maximum allowable levels of treatment and insecticide application, respectively. In numerical simulations, these upper bounds may be normalized to one. The objective functional is chosen to minimize infected plant biomass, pest density, and the relative control effort associated with the two interventions. Thus, the control problem is to find an optimal pair $(u_1^*, u_2^*) \in \mathcal{U}$ such that

$$\mathcal{J}(u_1^*, u_2^*) = \min_{(u_1,u_2)\in\mathcal{U}} \mathcal{J}(u_1, u_2) = \int_0^T \left[A_1 I(t) + A_2 V(t) + \frac{1}{2}\left(B_1 u_1^2(t) + B_2 u_2^2(t)\right)\right] dt, \tag{5.3}$$

The constants $A_1 \ge 0$ and $A_2 \ge 0$ measure the relative importance of reducing infected plant biomass and pest density, respectively. The constants $B_1 > 0$ and $B_2 > 0$ represent the relative weights assigned to the effort associated with treatment and insecticide application. The weights used in the numerical experiments are selected for illustrative purposes and are not calibrated from empirical agronomic or economic data. The relative weights assigned to intervention strategies can substantially influence the resulting control outcomes, highlighting the importance of interpreting intervention-based model predictions within the prescribed weighting structure [61]. Therefore, the numerical optimal control results are interpreted under the prescribed weighting structure and should not be regarded as a formal cost-effectiveness analysis. Different choices of the objective function weights may alter the optimal control profiles and the relative performance of the intervention strategies. Since the integrand is convex with respect to the control variables and the admissible control set is closed, convex, and bounded, standard optimal control arguments ensure the existence of an optimal control pair on the finite interval $[0, T]$.

To characterize the optimal controls, Pontryagin's minimum principle [62] is applied. Let $\lambda_1(t)$, $\lambda_2(t)$, and $\lambda_3(t)$ be the adjoint variables associated with $S(t)$, $I(t)$, and $V(t)$, respectively. The Hamilto-

nian is defined as

$$\begin{aligned}\mathcal{H} =& A_1 I + A_2 V + \frac{1}{2}\left(B_1 u_1^2 + B_2 u_2^2\right) \\ &+ \lambda_1 \left[rS\left(1 - \frac{S+I}{K}\right) - (\beta_L I + \beta_T V) S - a_S S V + u_1 I\right] \\ &+ \lambda_2 \left[(\beta_L I + \beta_T V) S - a_I I V - d_I I - u_1 I\right] \\ &+ \lambda_3 \left[c_S S V + c_I I V - d_V V - u_2 V\right],\end{aligned} \tag{5.4}$$

The adjoint equations are obtained from $\frac{d\lambda_j}{dt} = -\frac{\partial \mathcal{H}}{\partial x_j}$, $x_j \in \{S, I, V\}$. Therefore, the adjoint system is

$$\begin{aligned}\frac{d\lambda_1}{dt} =& -\lambda_1 \left[r\left(1 - \frac{2S+I}{K}\right) - \beta_L I - (\beta_T + a_S) V\right] - \lambda_2 (\beta_L I + \beta_T V) - \lambda_3 c_S V, \\ \frac{d\lambda_2}{dt} =& -A_1 - \lambda_1 \left[-\frac{rS}{K} - \beta_L S + u_1\right] - \lambda_2 \left[\beta_L S - a_I V - d_I - u_1\right] - \lambda_3 c_I V, \\ \frac{d\lambda_3}{dt} =& -A_2 + \lambda_1 (\beta_T + a_S) S - \lambda_2 (\beta_T S - a_I I) - \lambda_3 \left[c_S S + c_I I - d_V - u_2\right],\end{aligned} \tag{5.5}$$

Since no terminal cost is included and the final states are free, the transversality conditions are

$$\lambda_1(T) = 0, \qquad \lambda_2(T) = 0, \qquad \lambda_3(T) = 0, \tag{5.6}$$

The optimal controls are obtained from the stationarity conditions $\frac{\partial \mathcal{H}}{\partial u_1} = 0$ and $\frac{\partial \mathcal{H}}{\partial u_2} = 0$. From the Hamiltonian (5.4), the terms involving u_1 are $\frac{1}{2} B_1 u_1^2 + \lambda_1 u_1 I - \lambda_2 u_1 I$. Thus $\frac{\partial \mathcal{H}}{\partial u_1} = B_1 u_1 + \lambda_1 I - \lambda_2 I$. For an interior optimum, this gives $B_1 u_1 + \lambda_1 I - \lambda_2 I = 0$ or, equivalently, $u_1 = \frac{(\lambda_2 - \lambda_1) I}{B_1}$. Since the control must satisfy $0 \le u_1(t) \le u_{1,\max}$, the optimal treatment control is obtained by projecting the above expression onto the admissible interval. To avoid confusion with the coexistence equilibrium $E_3 = (S^*, I^*, V^*)$, the optimal state variables are denoted as $(\bar{S}(t), \bar{I}(t), \bar{V}(t))$. Hence, we have

$$u_1^*(t) = \min\left\{u_{1,\max}, \max\left\{0, \frac{(\lambda_2(t) - \lambda_1(t))\bar{I}(t)}{B_1}\right\}\right\}, \tag{5.7}$$

Similarly, the terms involving u_2 in the Hamiltonian are $\frac{1}{2} B_2 u_2^2 - \lambda_3 u_2 V$. Therefore, $\frac{\partial \mathcal{H}}{\partial u_2} = B_2 u_2 - \lambda_3 V$. For an interior optimum, $B_2 u_2 - \lambda_3 V = 0$, so that $u_2 = \frac{\lambda_3 V}{B_2}$. After projection onto the admissible interval $0 \le u_2(t) \le u_{2,\max}$, the optimal insecticide control is

$$u_2^*(t) = \min\left\{u_{2,\max}, \max\left\{0, \frac{\lambda_3(t)\bar{V}(t)}{B_2}\right\}\right\}. \tag{5.8}$$

Therefore, the optimality system consists of the controlled state system (5.1), the adjoint system (5.5), the transversality conditions (5.6), and the control characterizations (5.7)–(5.8). This system forms a two-point boundary value problem, since the state variables are prescribed at the initial time, whereas the adjoint variables satisfy terminal conditions at $t = T$. For the numerical implementation, the system is solved using a forward–backward sweep method until the state variables, adjoint variables, and control functions converge.

5.2. Controlled numerical scenarios

Numerical experiments were conducted to evaluate the performance of three intervention scenarios: Treatment only, insecticide only, and a combined treatment–insecticide strategy. The calculations were run over the time interval $0 \le t \le T$, with $T = 300$ and initial conditions $X_0 = (40, 10, 5)$. The parameter values listed in Table 4 were chosen to place the uncontrolled system in an oscillatory state, allowing the control strategies to be assessed under persistent fluctuations in disease pest dynamics.

The weights in the objective functional are chosen as $A_1 = 10$, $A_2 = 80$, $B_1 = 10$, and $B_2 = 10$. The objective functional is decomposed as $\mathcal{J} = \mathcal{J}_{A1} + \mathcal{J}_{A2} + \mathcal{J}_B$, where $\mathcal{J}_{A1} = \int_0^T A_1 I(t)\,dt$ measures the cumulative relative importance of infected plant biomass, $\mathcal{J}_{A2} = \int_0^T A_2 V(t)\,dt$ measures the cumulative relative importance of pest density, and $\mathcal{J}_B = \int_0^T \frac{1}{2}\left(B_1 u_1^2(t) + B_2 u_2^2(t)\right)\,dt$ represents the weighted cumulative control effort associated with treatment and insecticide application.

The selection of these weights reflects the relative priorities adopted for the numerical experiments. The larger value of A_2 assigns greater weight to reducing pest density because the pest population contributes both to plant damage through herbivory and to disease transmission through the vector-mediated pathway. Meanwhile, $A_1 = 10$ assigns positive weight to reducing infected plant biomass so that disease suppression remains part of the control objective. The control effort weights are set equally, $B_1 = B_2 = 10$, so that neither intervention is preferentially penalized through its corresponding weight. As stated above, these weights are selected for illustrative purposes and are not derived from empirical agronomic or economic cost data.

Table 5. Numerical summary of the optimal control strategies.

Strategy	$\mathcal{J}$	$\mathcal{J}_{A1}$	$\mathcal{J}_{A2}$	$\mathcal{J}_B$
No control	158755.7664	30471.0595	128284.7069	0
Treatment only	139301.8277	17743.6554	120856.5685	701.6039
Insecticide only	102091.0743	101097.2599	538.8204	454.9940
Combined control	1559.9120	241.9087	420.3993	897.6040

5.2.1. Treatment-only strategy

The treatment-only strategy for infected plants is shown in Figure 13, where $u_1^*(t)$ is applied and $u_2^*(t) = 0$. This strategy treats infected plants, thereby increasing the biomass of susceptible plants.

The results in Table 5 show that the weighted cumulative infected plant burden decreased from $30,471.0595$ without control to $17,743.6554$ under the treatment-only strategy, corresponding to a reduction of approximately 41.77%. However, the weighted cumulative pest burden decreased only from $128,284.7069$ to $120,856.5685$, or approximately 5.79%. This limited reduction is expected because no insecticide control is applied directly to the pest population. Consequently, pest density remains relatively high and the vector-mediated infection term $\beta_T VS$ remains active.

This strategy has a control effort contribution of 701.6039 and reduces the total objective value from 158755.7664 to 139301.8277, which is equivalent to an objective reduction of approximately 12.25%.

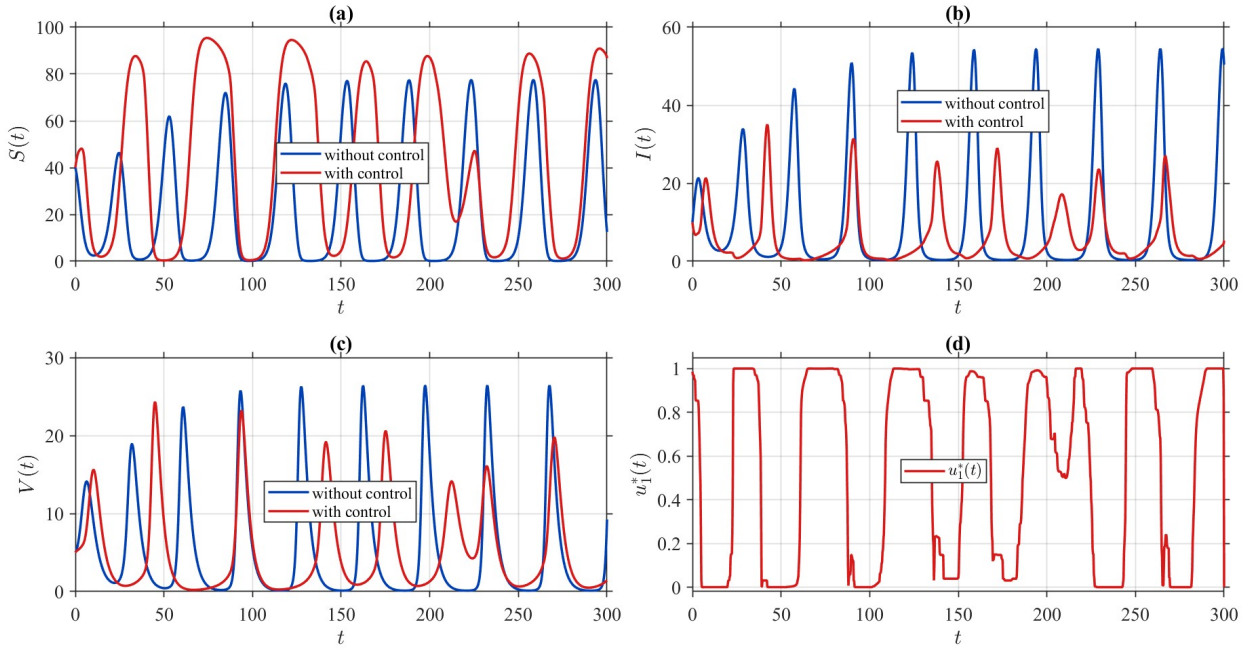


Figure 13. State variables and optimal control profile for the treatment-only strategy: (a) Susceptible plant biomass, (b) infected plant biomass, (c) pest density, and (d) optimal treatment control.

5.2.2. Insecticide-only strategy

An insecticide-only strategy, where $u_2^*(t)$ is applied while $u_1^*(t) = 0$, is implemented, as shown in Figure 14. This strategy suppresses pest density and reduces fluctuations in susceptible plant biomass, but it does not directly treat infected plants.

Table 5 shows that the weighted cumulative pest burden decreases from $128,284.7069$ without control to 538.8204 under the insecticide-only strategy. This confirms the strong suppression of pest density under the prescribed weighting structure. In contrast, the weighted cumulative infected plant burden increases from $30,471.0595$ to $101,097.2599$. Because $u_1^*(t) = 0$, no treatment-induced recovery is applied to infected plant biomass, while direct plant-to-plant transmission through $\beta_L S I$ remains active. Thus, suppressing the pest population alone does not necessarily suppress the infected plant burden when direct transmission persists.

The insecticide-only strategy has a control effort contribution of $\mathcal{J}_B = 454.9940$, which is lower than that of the other control strategies. However, the total objective value remains large, $\mathcal{J} = 102091.0743$, primarily because of the large weighted cumulative infected plant burden under this strategy.

5.2.3. Combined control strategy

The combined control strategy employs both treatment $u_1^*(t)$ and insecticide $u_2^*(t)$, as shown in Figure 15. Under this strategy, susceptible plant biomass increases rapidly toward the carrying capacity, with $S(T) = 99.9997 \approx K$.

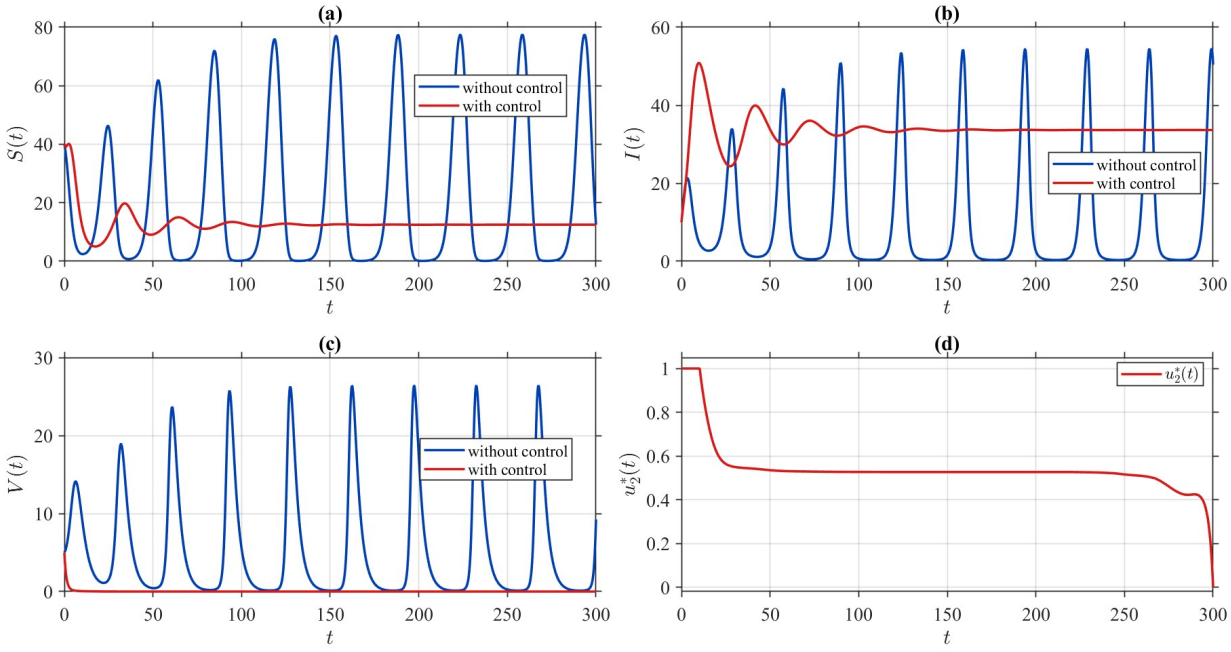


Figure 14. State variables and optimal control profile for the insecticide-only strategy: (a) Susceptible plant biomass, (b) infected plant biomass, (c) pest density, and (d) optimal insecticide control.

The results in Table 5 show that the weighted cumulative infected plant burden decreases from 30, 471.0595 in the uncontrolled case to 241.9087 under combined control. Similarly, the weighted cumulative pest burden decreases from 128, 284.7069 to 420.3993. Thus, for the selected parameter values, control bounds, and objective function weights, the combined strategy simultaneously produces substantial reductions in both infected plant biomass and pest density.

Among the three intervention scenarios, the combined strategy has the largest control effort contribution, with $\mathcal{J}_B = 897.6040$. At the same time, it produces substantial reductions in both biological components of the objective functional. Consequently, under the prescribed weights, the total objective value decreases from $\mathcal{J} = 158755.7664$ in the uncontrolled case to $\mathcal{J} = 1559.9120$ under combined control.

Therefore, for the selected parameter values, control bounds, and objective function weights, the combined treatment–insecticide strategy provides the strongest simultaneous suppression of infected plant biomass and pest density among the three intervention scenarios considered. However, this result should not be interpreted as establishing the general practical superiority of the combined strategy. The combined control problem has a larger admissible control set than either single-control problem, and its numerical performance depends on the prescribed objective function weights. Thus, the comparison is specific to the control formulation and numerical setting considered in this study.

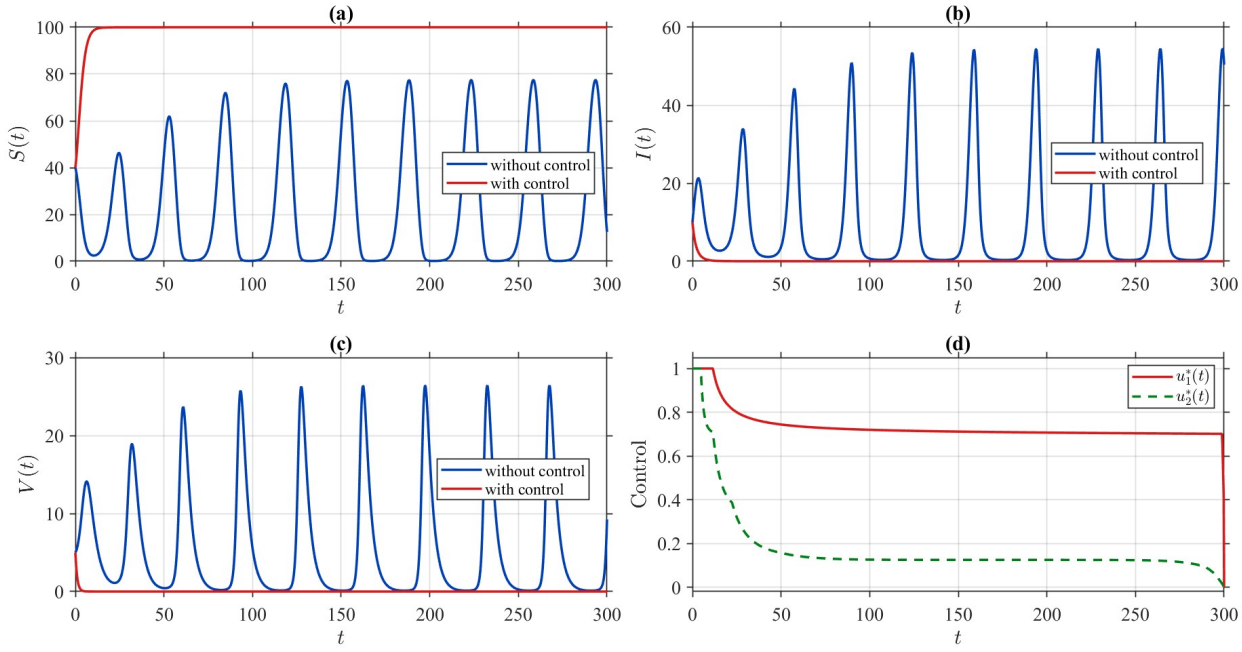


Figure 15. State variables and optimal control profiles for the combined control strategy: (a) Susceptible plant biomass, (b) infected plant biomass, (c) pest density, and (d) optimal treatment and insecticide controls.

6. Conclusions

The proposed eco-epidemiological plant–pest model was shown to be well-posed in the biologically feasible region, with non-negative and bounded solutions. The equilibrium and threshold analyses characterized the invasion conditions and local stability of the plant-only, pest-free infected, and coexistence equilibria. Under the stated threshold conditions, uniform persistence was established. Furthermore, the Li–Muldowney geometric approach yielded a conditional contraction criterion for the second additive compound system, providing a sufficient condition for excluding non-trivial periodic orbits under the applicable geometric hypotheses. The bifurcation analysis identified a transcritical transition at $\mathcal{R}_I = 1$ and a codimension-two double-zero threshold interaction at $\mathcal{R}_I = \mathcal{R}_V^{(1)} = 1$. A Hopf bifurcation with respect to pest mortality d_V was established analytically under the required conditions, while numerical investigations revealed oscillatory transitions associated with d_V and vector-mediated transmission β_T. For the selected parameter set, the Hopf bifurcation with respect to β_T was supercritical.

The results highlight the roles of direct and vector-mediated transmission, pest mortality, and allomone-mediated suppression in shaping long-term system dynamics. The LHS–PRCC analysis identified β_L and d_I as influential parameters for mean susceptible plant biomass, K for mean infected plant biomass, and d_V for mean pest density. Numerical simulations indicated that vector-mediated transmission can promote sustained oscillations, whereas allomone-mediated suppression can reduce pest density and favor stable coexistence. Under the selected objective function weights and control bounds, the combined treatment–insecticide strategy produced the greatest reduction in infected plant

biomass and pest density among the strategies considered. These findings support further investigation of integrated plant treatment, pest suppression, and allomone-based management, particularly with empirically calibrated parameters and intervention costs.

Future research may extend the model by incorporating natural enemies, volatile organic compound mediated attraction of natural enemies, and explicitly distinguishing between uninfected and infected pest populations. Such extensions would allow a more detailed investigation of pathogen transmission, pest–natural enemy interactions, and their effects on invasion thresholds, stability, and bifurcation dynamics.

Use of AI tools declaration

The authors declare they have not used artificial intelligence (AI) tools in the creation of this article.

Acknowledgments

The authors gratefully acknowledge the financial support provided by the Indonesia Endowment Fund for Education Agency (LPDP), Ministry of Finance of the Republic of Indonesia, in supporting this research.

Conflict of interest

The authors declare there is no conflict of interest.

References

1. J. Pretty, Z. P. Bharucha, Integrated pest management for sustainable intensification of agriculture in Asia and Africa, *Insects*, **6** (2015), 152–182. https://doi.org/10.3390/insects6010152
2. S. Engindeniz, G. O. Cosar, An economic comparison of pesticide applications for processing and table tomatoes: A case study for Turkey, *J. Plant Prot. Res.*, **53** (2013), 230–237. https://doi.org/10.2478/jppr-2013-0035
3. M. Love, R. D. Magarey, B. L. Holderman, D. S. Carley, F. Maggi, N. Singer, Tracking sustainability in crop pest management in the United States using an eco-efficiency index, *Front. Insect Sci.*, **5** (2025), 1582496. https://doi.org/10.3389/finsc.2025.1582496
4. I. Tlak Gajger, S. A. Dar, Plant allelochemicals as sources of insecticides, *Insects*, **12** (2021), 189. https://doi.org/10.3390/insects12030189
5. R. A. Schmidt-Jeffris, Nontarget pesticide impacts on pest natural enemies: Progress and gaps in current knowledge, *Curr. Opin. Insect Sci.*, **58** (2023), 101056. https://doi.org/10.1016/j.cois.2023.101056
6. R. Kaur, D. Choudhary, S. Bali, S. S. Bandral, V. Singh, M. A. Ahmad, et al., Pesticides: An alarming detrimental to health and environment, *Sci. Total Environ.*, **915** (2024), 170113. https://doi.org/10.1016/j.scitotenv.2024.170113

7. M. Jeger, The epidemiology of plant virus disease: Towards a new synthesis, *Plants*, **9** (2020), 1768. https://doi.org/10.3390/plants9121768
8. M. P. Daugherty, J. R. S. Lopes, R. P. P. Almeida, Vector within-host feeding preference mediates transmission of a heterogeneously distributed pathogen, *Ecol. Entomol.*, **35** (2010), 360–366. https://doi.org/10.1111/j.1365-2311.2010.01189.x
9. R. Donnelly, C. A. Gilligan, The role of pathogen-mediated insect superabundance in the East African emergence of a plant virus, *J. Ecol.*, **110** (2022), 1113–1124. https://doi.org/10.1111/1365-2745.13854
10. M. Jeger, F. Hamelin, N. J. Cunniffe, Emerging themes and approaches in plant virus epidemiology, *Phytopathology*, **113** (2023), 1630–1646. https://doi.org/10.1094/PHYTO-10-22-0378-V
11. A. E. Whitfield, B. W. Falk, D. Rotenberg, Insect vector-mediated transmission of plant viruses, *Virology*, **479–480** (2015), 278–289. https://doi.org/10.1016/j.virol.2015.03.026
12. P. A. Divekar, N. Srinivasa, B. A. Divekar, R. Kumar, G. B. Gowda, A. Ray, et al., Plant secondary metabolites as defense tools against herbivores for sustainable crop protection, *Int. J. Mol. Sci.*, **23** (2022), 2690. https://doi.org/10.3390/ijms23052690
13. W. D. J. Kirk, W. J. de Kogel, E. H. Koschier, D. A. J. Teulon, Semiochemicals for thrips and their use in pest management, *Annu. Rev. Entomol.*, **66** (2021), 101–119. https://doi.org/10.1146/annurev-ento-022020-081531
14. M. Parashar, M. Rathinam, N. Dokka, R. Sreevathsa, Chemical camouflage in plants: Defensive science of stealth against insect herbivory, *ACS Agric. Sci. & Technol.*, **5** (2025), 1251–1262. https://doi.org/10.1021/acsagscitech.5c00223
15. N. M. A. El-Ghany, Pheromones and chemical communication in insects, in *Pests, Weeds and Diseases in Agricultural Crop and Animal Husbandry Production* (eds. D. Kontogiannatos, A. Kourti and K.F. Mendes), IntechOpen, London, (2020). https://doi.org/10.5772/intechopen.92384
16. J. Poldy, Volatile cues influence host-choice in arthropod pests, *Animals*, **10** (2020), 1984. https://doi.org/10.3390/ani10111984
17. H. A. F. El-Shafie, J. R. Faleiro, Semiochemicals and their potential use in pest management, in *Biological Control of Pest and Vector Insects* (ed. V.D.C. Shields), IntechOpen, London, (2017). https://doi.org/10.5772/66463
18. J. Boevé, R. Giot, Chemical composition: Hearing insect defensive volatiles, *Patterns*, **2** (2021), 100352. https://doi.org/10.1016/j.patter.2021.100352
19. S. J. Seybold, C. J. Fettig, Managing bark and ambrosia beetles (Coleoptera: Curculionidae: Scolytinae) with semiochemicals, *Can. Entomol.*, **153** (2020), 4–12. https://doi.org/10.4039/tce.2020.24
20. J. N. Haro-González, G. A. Castillo-Herrera, M. Martínez-Velázquez, H. Espinosa-Andrews, Clove essential oil (*Syzygium aromaticum* L. Myrtaceae): Extraction, chemical composition, food applications, and essential bioactivity for human health, *Molecules*, **26** (2021), 6387. https://doi.org/10.3390/molecules26216387

21. T. A. W. Asnan, S. Widayanti, I. S. Harahap, H. Widhisatuti, The effectiveness of clove oil, its fractions, and clove oil-based fumigant tablet formulations, against *Tribolium castaneum* (Herbst), *J. Entomol. Indones.*, **18** (2021), 191. https://doi.org/10.5994/jei.18.3.191
22. M. A. Ullah, A. Hassan, A. Hamza, Role of clove in human medical history, *SAR J. Anat. Physiol.*, **4** (2023), 10–19. https://doi.org/10.36346/sarjap.2023.v04i02.001
23. B. C. D. Jorge, H. E. Hummel, J. Groß, Repellent activity of clove essential oil volatiles and development of nanofiber-based dispensers against pear psyllids (Hemiptera: Psyllidae), *Insects*, **13** (2022), 743. https://doi.org/10.3390/insects13080743
24. S. Chaudhary, R. K. Kanwar, A. Sehgal, D. M. Cahill, C. J. Barrow, R. Sehgal, et al., Progress on *Azadirachta indica* based biopesticides in replacing synthetic toxic pesticides, *Front. Plant Sci.*, **8** (2017), 610. https://doi.org/10.3389/fpls.2017.00610
25. S. Chaudhary, S. K. Yadav, P. Verma, S. Sagar, M. Lal, Botanical insecticides for crop protection: Major classes and possible mechanisms of action, in *Insecticides in Pest Control - Impact, Challenges and Strategies* (ed. S. Kumar), IntechOpen, (2024). https://doi.org/10.5772/intechopen.1006743
26. F. Acheuk, S. Basiouni, A. A. Shehata, K. Dick, H. Hajri, S. Lasram, et al., Status and prospects of botanical biopesticides in Europe and Mediterranean countries, *Biomolecules*, **12** (2022), 311. https://doi.org/10.3390/biom12020311
27. J. M. Grunseich, M. N. Thompson, N. M. Aguirre, A. M. Helms, The role of plant-associated microbes in mediating host-plant selection by insect herbivores, *Plants*, **9** (2019), 6. https://doi.org/10.3390/plants9010006
28. K. E. Mauck, C. M. de Moraes, M. C. Mescher, Deceptive chemical signals induced by a plant virus attract insect vectors to inferior hosts, *Proc. Natl. Acad. Sci. U.S.A.*, **107** (2010), 3600–3605. https://doi.org/10.1073/pnas.0907191107
29. S. M. Nebapure, K. Shankarganesh, S. Rajna, K. C. Naga, D. Pandey, S. Gambhir, et al., Dynamic changes in virus-induced volatiles in cotton modulate the orientation and oviposition behavior of the whitefly *Bemisia tabaci*, *Front. Physiol.*, **13** (2022), 1017948. https://doi.org/10.3389/fphys.2022.1017948
30. X. Martini, M. R. Coy, E. H. Kuhns, L. L. Stelinski, Temporal decline in pathogen-mediated release of methyl salicylate associated with decreasing vector preference for infected over uninfected plants, *Front. Ecol. Evol.*, **6** (2018), 185. https://doi.org/10.3389/fevo.2018.00185
31. X. Chang, Y. Guo, Y. Ren, Y. Li, F. Wang, G. Ye, et al., Virus-induced plant volatiles promote virus acquisition and transmission by insect vectors, *Int. J. Mol. Sci.*, **24** (2023), 1777. https://doi.org/10.3390/ijms24021777
32. M. S. Ullah, E. Hernández-López, J. Wang, Nonlinear dynamics and memory effects of an eco-epidemiological model: a bifurcation study with Allee thresholds and behavioral feedback, *Model. Earth Syst. Environ.*, **12** (2025). https://doi.org/10.1007/s40808-025-02628-0
33. N. Sk, B. Mondal, M. Ch-Chaoui, R. K. Upadhyay, S. Mandal, P. K. Tiwari, Influence of Allee effect and cooperative hunting on the dynamics of a modified Hastings–Powell model in deterministic, discrete, and stochastic environments, *Eur. Phys. J. Plus*, **140** (2025), 1178. https://doi.org/10.1140/epjp/s13360-025-07123-0

34. M. J. Jeger, J. Holt, F. van den Bosch, L. V. Madden, Epidemiology of insect-transmitted plant viruses: Modelling disease dynamics and control interventions, *Physiol. Entomol.*, **29** (2004), 291–304. https://doi.org/10.1111/j.0307-6962.2004.00394.x

35. R. Shi, H. Zhao, S. Tang, Global dynamic analysis of a vector-borne plant disease model, *Adv. Differ. Equ.*, **2014** (2014), 59. https://doi.org/10.1186/1687-1847-2014-59

36. V. A. Bokil, L. J. S. Allen, M. J. Jeger, S. Lenhart, Optimal control of a vectored plant disease model for a crop with continuous replanting, *J. Biol. Dyn.*, **13** (2019), 325–353. https://doi.org/10.1080/17513758.2019.1622808

37. R. Mondal, D. Kesh, D. Mukherjee, Influence of induced plant volatile and refuge in tritrophic model, *Energy Ecol. Environ.*, **3** (2018), 171–184. https://doi.org/10.1007/s40974-018-0092-0

38. C. Sun, M. Loreau, Dynamics of a three-species food chain model with adaptive traits, *Chaos Solitons & Fractals*, **41** (2009), 2812–2819. https://doi.org/10.1016/j.chaos.2008.10.015

39. R. Mondal, Y. Takeuchi, D. Kesh, D. Mukherjee, Dynamical study on volatiles signaling in plant disease and pest-natural enemy interaction, *Model. Earth Syst. Environ.*, **11** (2025), 57. https://doi.org/10.1007/s40808-024-02248-0

40. G. Thomas, Q. Rusman, W. R. Morrison III, D. M. Magalhães, J. A. Dowell, E. Ngumbi, et al., Deciphering plant-insect-microorganism signals for sustainable crop production, *Biomolecules*, **13** (2023), 997. https://doi.org/10.3390/biom13060997

41. N. M. Abd El-Ghany, Semiochemicals for controlling insect pests, *J. Plant Prot. Res.*, **59** (2019), 1–11. https://doi.org/10.24425/jppr.2019.126036

42. A. Sharma, R. K. Sandhi, G. V. P. Reddy, A review of interactions between insect biological control agents and semiochemicals, *Insects*, **10** (2019), 439. https://doi.org/10.3390/insects10120439

43. K. Yazaki, G. Arimura, T. Ohnishi, 'Hidden' terpenoids in plants: Their biosynthesis, localization and ecological roles, *Plant Cell Physiol.*, **58** (2017), 1615–1621. https://doi.org/10.1093/pcp/pcx123

44. G. M. Gurr, J. Liu, J. A. Pickett, P. C. Stevenson, Review of the chemical ecology of homoterpenes in arthropod–plant interactions, *Austral Entomol.*, **62** (2023), 3–14. https://doi.org/10.1111/aen.12629

45. L. Perko, *Differential Equations and Dynamical Systems*, 3^{rd} edition, Springer Science & Business Media, New York, 2013.

46. J. A. Oguntuase, On an inequality of Gronwall, *J. Inequal. Pure Appl. Math.*, **2** (2001), 6.

47. F. van den Bosch, M. J. Jeger, The basic reproduction number of vector-borne plant virus epidemics, *Virus Res.*, **241** (2017), 196–202. https://doi.org/10.1016/j.virusres.2017.06.014

48. R. Amelia, N. Anggriani, A. K. Supriatna, N. Istifadah, Mathematical model for analyzing the dynamics of tungro virus disease in rice: A systematic literature review, *Mathematics*, **10** (2022), 2944. https://doi.org/10.3390/math10162944

49. A.-F. O. Ayembillah, B. Seidu, C. S. Bornaa, Mathematical modeling of the dynamics of maize streak virus disease (MSVD), *Math. Model. Control*, **2** (2022), 153–164. https://doi.org/10.3934/mmc.2022016

50. R. Amelia, N. Anggriani, A. K. Supriatna, N. Istifadah, Analysis and optimal control of the tungro virus disease spread model in rice plants by considering the characteristics of the virus, roguing, and pesticides, *Mathematics*, **11** (2023), 1151. https://doi.org/10.3390/math11051151
51. S. T. Tresna, N. Anggriani, A. K. Supriatna, Study of mathematical modeling for plant disease transmission: A systematic literature review during 2012–2022, *Jambura J. Biomath.*, **4** (2023), 1–14. https://doi.org/10.34312/jjbm.v4i1.18443
52. J. D. Murray, *Mathematical Biology I: An Introduction*, 3^{rd} edition, Springer-Verlag, New York, 2002.
53. H. I. Freedman, P. Waltman, Persistence in models of three interacting predator-prey populations, *Math. Biosci.*, **68** (1984), 213–231. https://doi.org/10.1016/0025-5564(84)90032-4
54. M. Y. Li, J. S. Muldowney, On Bendixson's criterion, *J. Differ. Equ.*, **106** (1993), 27–39. https://doi.org/10.1006/jdeq.1993.1097
55. M. Y. Li, J. S. Muldowney, A geometric approach to global-stability problems, *SIAM J. Math. Anal.*, **27** (1996), 1070–1083. https://doi.org/10.1137/S0036141094266449
56. C. Robinson, *An Introduction to Dynamical Systems: Continuous and Discrete*, 2^{nd} edition, American Mathematical Society, Providence, RI, 2012.
57. S. Marino, I. B. Hogue, C. J. Ray, D. E. Kirschner, A methodology for performing global uncertainty and sensitivity analysis in systems biology, *J. Theor. Biol.*, **254** (2008), 178–196. https://doi.org/10.1016/j.jtbi.2008.04.011
58. C. Dai, Z. Wang, W. Wang, Y. Li, K. Wang, Epidemics and underlying factors of multiple-peak pattern on hand, foot and mouth disease in Wenzhou, China, *Math. Biosci. Eng.*, **16** (2019), 2168–2188. https://doi.org/10.3934/mbe.2019106
59. F. B. Agusto, E. Numfor, K. Srinivasan, E. A. Iboi, A. Fulk, J. M. Saint Onge, et al., Impact of public sentiments on the transmission of COVID-19 across a geographical gradient, *PeerJ*, **11** (2023), e14736. https://doi.org/10.7717/peerj.14736
60. M. A. Khan, Z. U. A. Zafar, I. Ahmad, N. M. Isa, E. Alzahrani, Numerical modeling and simulation of stochastic fractional order model for COVID-19 infection in Mittag–Leffler kernel, *Sci. Rep.*, **15** (2025), 33031. https://doi.org/10.1038/s41598-025-18513-w
61. M. S. Ullah, X. Wang, J. Wang, A cost-sensitive behavioral modeling analysis of the early identification and control of infectious diseases, *Bull. Math. Biol.*, **88** (2026), 129. https://doi.org/10.1007/s11538-026-01696-2
62. S. Lenhart, J.T. Workman, *Optimal Control Applied to Biological Models*, Chapman & Hall/CRC, Boca Raton, 2007. https://doi.org/10.1201/9781420011418



AIMS Press

© 2026 the Author(s), licensee AIMS Press. This is an open access article distributed under the terms of the Creative Commons Attribution License (https://creativecommons.org/licenses/by/4.0)